Thermo-Mechanical Modeling of a Micro-Fabricated Solid Oxide Fuel Cell

by

Tze Yung Andrew Ie
Sc. B. Brown University(2001)

Submitted to the Department of Aeronautics and Astronautics
in partial fulfillment of the requirements for the degree of

Master of Science

at the

MASSACHUSETTS INSTITUTE OF TECHNOLOGY

June 2004

Author .....
Department of Aeronautics and Astronautics
March, 2004

Certified by .....
S. Mark Spearing
Associate Professor
Thesis Supervisor

Accepted by .....
Edward M. Greitzer
H. N. Slater Professor of Aeronautics and Astronautics, Chair,
Committee on Graduate Students

AERO

Thermo-Mechanical Modeling of a Micro-Fabricated Solid Oxide Fuel Cell

by

Tze Yung Andrew Ie

Sc. B. Brown University(2001)

Submitted to the Department of Aeronautics and Astronautics
on March, 2004, in partial fulfillment of the
requirements for the degree of
Master of Science

Abstract

A micro-fabricated solid oxide fuel cell is currently being designed by the Microchemical Power Team(funded under the Multidisciplinary University Research Initiative(MURI) Research Program). In the current design a plate structure vital to power generation is exposed to harsh thermal operation conditions, making it susceptible to structural failure. This thesis investigates the mechanisms of its structural failure, develops tools and models to understand the mechanisms quantitatively, and gives suggestions to guide the design process with the models developed.
The thesis begins with a brief overview of the principles of fuel cell operation, their associated operating conditions, along with a description of how these conditions may lead to structural failure. Next a representative structure of a portion of a fuel cell critical to power generation is analyzed, for a given temperature distribution. Different temperature distributions across the same structure are also analyzed. Results from these analyses are then used to provide guidance for the design process. Finally future directions for research are given.

Thesis Supervisor: S. Mark Spearing
Title: Associate Professor

Acknowledgments

All attempts have been made to ensure the accuracy and completeness of the references for this thesis. If any references are mistakenly omitted, I sincerely apologize.
This thesis is made possible by the Department of Defense Multidisciplionary University Research Inititative(MURI) under Grant DAAD 19-01-1-05 66 U.S. given by the Army Research Office. I sincerely thank them for their support.
Next I would like to thank my advisor Professor S. Mark Spearing for his advice and guidance for my research and thesis.
Also I want to express my thanks to the colleagues in the MURI Research Group, Technology Laboratory for Advanced Composites, and many other individuals who have helped me to complete this thesis.
Finally this thesis is written in memory of my father, Ie It Sim, and in gratitude to my mother, Ie Khoo Ah Khim.

Contents

List of Figures

List of Tables

Chapter 1

Motivation and Aim

With the current push for clean power, combined with the demand for high power density (energy per unit mass) portable power, the microchemical power team composed of members from various departments at the Massachusetts Institute of Technology is currently exploring different fuel cell designs to meet this need.

Currently there are four types of fuel cells that are under widespread use, with their designs differing in the choice of their electrolytes. These different electrolytes are alkaline, acid, molten carbonate and solid oxide. Although these four types of electrolytes may be quite different in their designs, the fuel cells all generate electricity through a very similar mechanism. Fuel cells generate electricity by the *indirect* reaction between a fuel and an oxidant, where the indirect reaction occurs through an intermediate separation layer, or the electrolyte. The electrolyte is partially covered by electrodes, and these electrodes provide and capture electrons during the fuel/oxidant reaction. Overall this electron exchange process manifests itself as an electric current flowing in the circuit.

A desirable characteristic for a fuel cell is to have a high power to mass ratio, as this enables portability, and/or high power generation. One technique for increasing this ratio is by decreasing the mass of the fuel cell, while keeping the power generation constant. A considerable mass reduction can be achieved through Micro Electro-Mechanical Systems(MEMS) fabrication technology, since fuel cell features can be decreased to the micron-scale with accuracy and controllability. A solid oxide fuel

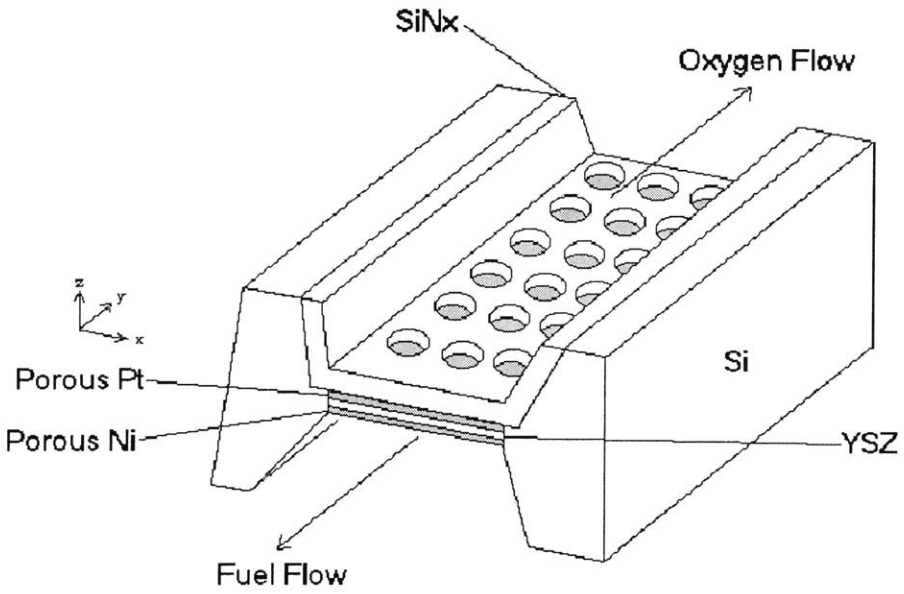

Figure 1-1: Design of SOFC Proposed by Baertsch *et al.*[3]

cell is suitable for MEMS fabrication, since it uses a solid electrolyte, therefore making it the easiest to fabricate and control [12, 25].

The most recent design of a micro-fabricated SOFC proposed by Baertsch *et al.* [3, 9, 2] is shown in Figure 1-1. The principle of operation of this device is as follows:

With fuel and oxygen flowing over opposite sides of the YSZ electrolyte plate structure, they react indirectly through the YSZ plate. Electrons are collected at the electrodes on the YSZ plate, generating a current. The area of the electrode governs the power generated for a given fuel/oxidant, temperature, and flow rate. Therefore the YSZ plate is central to power generation. For the fuel/oxidant reaction to occur, the YSZ plate must be heated up to temperatures of 500^0-1000^0C. Such high temperatures may prove to be structurally detrimental to the YSZ plate structure. For example, during heating up of the plate structure, if the coefficient of thermal expansion (CTE) of the substrate is smaller than that of the electrolyte, then the electrolyte plate structure would expand more than the surrounding substrate. This will translate to the generation of in-plane compressive stresses within the electrolyte plate, possibly leading to its buckling and therefore structural failure. Conversely,

during heat up, if the CTE of the substrate is larger than that of the electrolyte, in-plane tensile stresses will be generated, leading to possible failure by brittle fracture. Realizing that the structural failure of the plate structure hinders electrolyte operation and therefore power generation, the YSZ plate structure must be designed for prevention of structural failure. Yet it is equally unacceptable to over-design the structure, as over-designing will decrease fuel cell efficiency.

The aim of this thesis is to analyze the mechanics issues faced by the candidate fuel cell design. This consists of the following tasks: 1) Analyze structural stability of the YSZ plate under various temperature distributions, 2) Develop the necessary tools to analyze the stability and power generation capability of the YSZ structure, 3) Develop design maps for the YSZ structure to indicate possible design regions where failure could be avoided during the operation of the fuel cell, 4) Assess the power generation capability of the current design, determining whether it could generate sufficient power, or if a new design is needed for higher power generation.

The thesis is organized as follows. Chapter 2 provides an overview of the fuel cell power generation mechanism and outlines a possible fabrication route. Variables affecting YSZ fuel cell performance are described, and the mechanics of the structure in relation to them is presented. Chapter 3 analyzes the mechanics of the plate under a uniform temperature distribution. Power generation and heat loss under this temperature distribution are assessed for structurally stable plates. The necessary tools and design maps are derived for this temperature distribution. Chapter 4 explores the behavior of the plate when exposed to non-uniform temperature distributions. Tools are developed, and power generated and heat loss analyzed for these temperature distributions. Chapter 5 then compares the power generation capabilities of structurally stable plates for the different temperature distributions plate geometries, to observe whether one temperature distribution or geometry has an advantage over another. A conclusion is drawn as to whether there is a need for a completely different design. Finally Chapter 6 discusses possible topics for future investigations.

Chapter 2

Overview of Fuel Cell Design

An understanding of the operation mechanism, design variables affecting YSZ fuel cell power generation and the fabrication process is required to provide context for the results from the mechanics and power generation analyses of the fuel cell.

2.1 Operating Principles of the SOFC

A cross section of a generic SOFC is shown in Figure 2-1.

In the case at hand, the fuel is assumed to be hydrogen and the oxidant to be oxygen. The solid electrolyte is YSZ, with a porous anode and cathode on either side of the electrolyte. The YSZ electrolyte is first heated up to its active operation temperature(approximately 600^0-800^0C). At that temperature, oxygen obtains electrons from the cathode:

$$O_2 + 4e^- \leftrightharpoons 2O^{2-}$$

The oxygen ions then diffuse through the YSZ electrolyte, and the oxygen ions react with hydrogen molecules on the YSZ/anode interface [25, 12]:

$$2H_2 \leftrightharpoons 4e^- + 4H^+$$

The sum of the reactions is the formation of water, and the overall exchange of

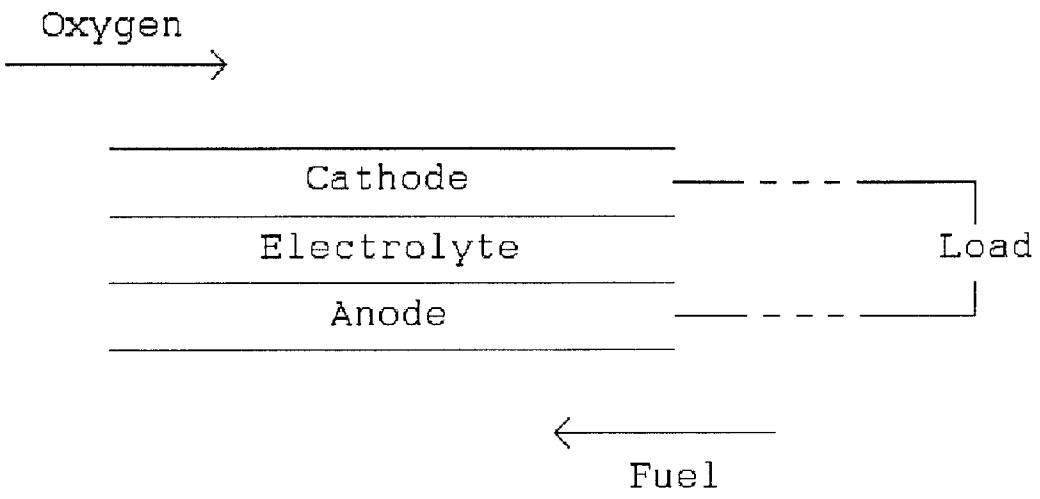

Figure 2-1: Generic SOFC Cross Section [25, 12]

electrons from one electrode to another manifests itself as an electrical current.

2.2 Transistion to Micro-Chemical Fuel Cell

The SOFC concept is translated to the micron scale through Micro Electro-Mechanical Systems(MEMS) fabrication technology. In the proposed design in Figure 1-1, YSZ is the solid electrolyte. On either side of the electrolyte are a platinum (Pt) anode and a nickel (Ni) cathode. A layer of silicon nitride (SiN_x) is deposited between the electrolyte and one of the electrodes (the exact structure is a design variable), and the whole composite plate structure is supported at its periphery by silicon(Si). Note that Si and SiN_x serve no direct part in the generation of electric power; Si is the underlying support for the entire structure, and the SiN_x is present to increase the stiffness of the YSZ layer.

It is anticipated that the YSZ will be operating at temperatures of 600^0-800^0C, and that there will be no pressure difference between the fuel and the oxygen. Other design variables are free for tuning to maximize fuel cell power generation capability. The design requirements that maximize power generation capability are presented in

the next section.

2.3 Design Requirements of the Micro-Chemical SOFC

Since the YSZ plate structure is responsible for ionic conduction and the overall power generation, different YSZ structure designs will affect the power generation capability of the fuel cell. The design requirements that ensures maximum power generation by the YSZ plate structure are as follows:

The process of ionization of oxygen molecules and their subsequent diffusion through the YSZ electrolyte begins at the YSZ/cathode interface. The rate at which this process occurs depends on the accessibility of the YSZ/cathode interfaces to the oxygen molecules. Similarly for the anode, the hydrogen molecules need to be able to reach and access the YSZ/anode interface to react with the oxygen ions, thereby completing the reaction and the electron transfer process. To increase the rate of both of these processes and therefore the overall power generation capability of the fuel cell, the area of the YSZ/electrode interface must be maximized. One way of achieving this would be to increase the porosity of the electrodes, but this will depend upon material fabrication and electrical function of the electrodes. Another technique for approaching the design requirement is to remove the SiN_x support layer to have effectively one large YSZ composite, as this would free up area available for oxygen transport [25, 12, 24]. Yet in turn this decreases the stiffness of the composite, making it more susceptible to buckling failure.

Returning to the oxygen ion diffusion through the YSZ structure, the rate for this process to occur and the overall power generated will be increased if the thickness of the YSZ plate structure is decreased. This is due to the higher ionic conductivity from a thinner YSZ plate.

Finally the YSZ plate structure is heated by resistive wires to temperatures of 600^0-800^0C. The large temperature difference between the plate temperature and the am-

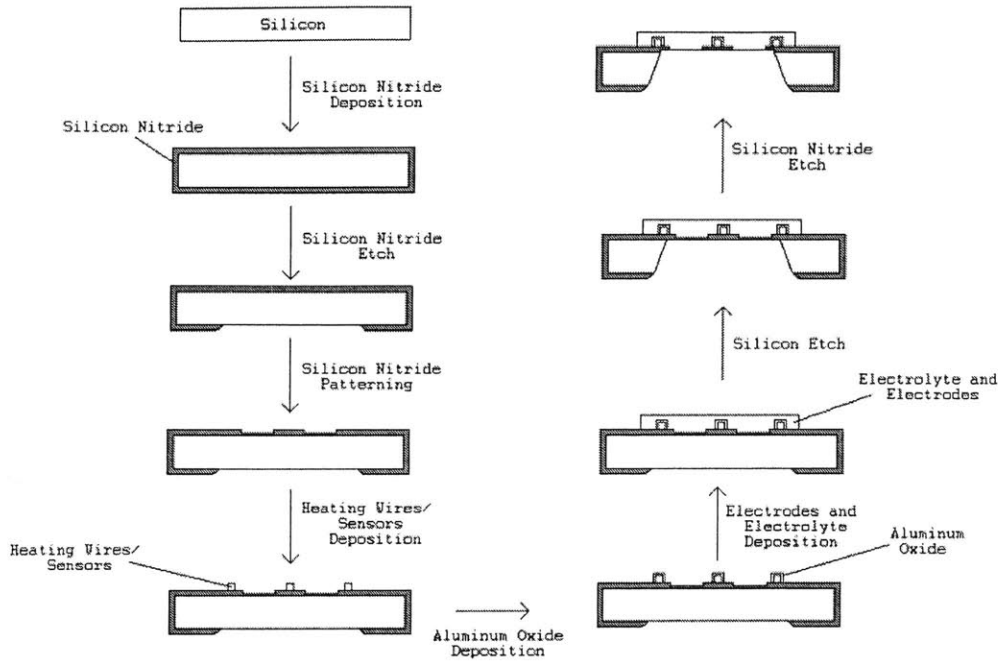

Figure 2-2: Fabrication Steps of a Microchemical SOFC [4, 3]

bient temperature would drive heat out of the device, hence decreasing the net power generated. The design requirement from this concern is therefore to minimize heat loss out of the YSZ structure.

2.4 Fabrication of Micro-Chemical SOFC

The proposed fuel cell design presented in Figure 1-1 is realized through the fabrication steps proposed by Baertsch [4, 3] as shown in Figure 2-2.

Starting out with a silicon wafer, a layer of silicon nitride is deposited. Next the silicon nitride on one side of the wafer is partially etched away. To make openings for the free-standing YSZ, the remaining unetched side is etched in a manner showed in Figure 2-2. Heating wires and temperature sensors are deposited on one side of the wafer. Next a layer of aluminum oxide is deposited on top of the wires and sensors to increase heat insulation. An electrode layer, a YSZ layer, and another electrode layer are then deposited over the silicon nitride and the insulated wires. Finally to release

the YSZ free-standing plates, the silicon and the silicon nitride layer are etched away.

2.5 Mechanisms for Structural Failure of Micro-Chemical SOFC

The fabricated Micro-Chemical SOFC is susceptible to structural failure through various combinations of the following operation and loading conditions:

1. Temperature gradients
2. Absolute Temperatures
3. CTE mismatch between different materials
4. Residual stresses of different materials, developed during their fabrication
5. Long term temperature fluctuations

Four failure modes could occur due to the above conditions: The two failure modes that require a long time-frame to occur are creep and fatigue, and the other two are fracture and buckling.

Creep ensues when the material is under stress for a long period of time, and simultaneously exposed to a temperature in excess of approximately 1/3 of its melting temperature [20]. Compressive stresses developed through the operation and loading conditions could cause creep buckling, and tensile stresses could lead to creep fracture [27]. Fatigue is a failure mode that also occurs over a long time frame, but this failure mode is characterized by the plate being exposed to fluctuating stresses over time, caused by fluctuating operation and loading conditions. Since this project is currently in the trial device fabrication stage, these two failure modes are disregarded in this thesis.

The failure modes that require immediate attention at this stage of device development are fracture and and buckling.

Fracture is caused by large tensile stresses within the plate structure. These tensile

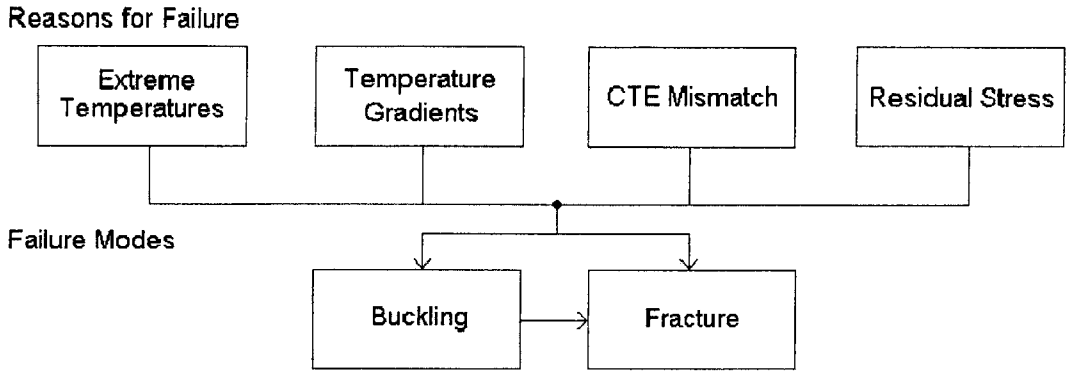

Figure 2-3: Flow Chart of Reasons for Failure, and Resulting Failure Modes

stresses could either be initially present in form of residual stress, or they could be generated through operation and/or loading conditions such as temperature gradients, CTE mismatches, and temperature changes. Buckling is also caused by residual stresses, temperature gradients, CTE mismatches and temperature changes, but in this failure mode the stresses within the plate are compressive.

Considering only failure modes pertinent to this fuel cell development stage, fracture of the YSZ plate structure is most detrimental to the fuel cell. This is because fracture of the electrolyte would allow direct mixing of fuel and oxygen, giving way to a possible explosion. Although buckling does not directly affect electrolyte function since this failure mode only results in electrolyte out-of-plane deformation, significant bending stresses may develop in the YSZ structure due to this new configuration, leading to fracture. Therefore both failure modes must be avoided to ensure fuel cell structural stability.

2.6 Preventative Measures for Structural Failure, and Their Impact on Design Requirements

Figure 2-4 shows the relation between failure modes and their preventative measures, and how these preventative measures in turn affect the design requirements.

To illustrate the use of this figure, consider the buckling failure mode. This failure mode could be prevented by increasing the thickness and/or decreasing the side length

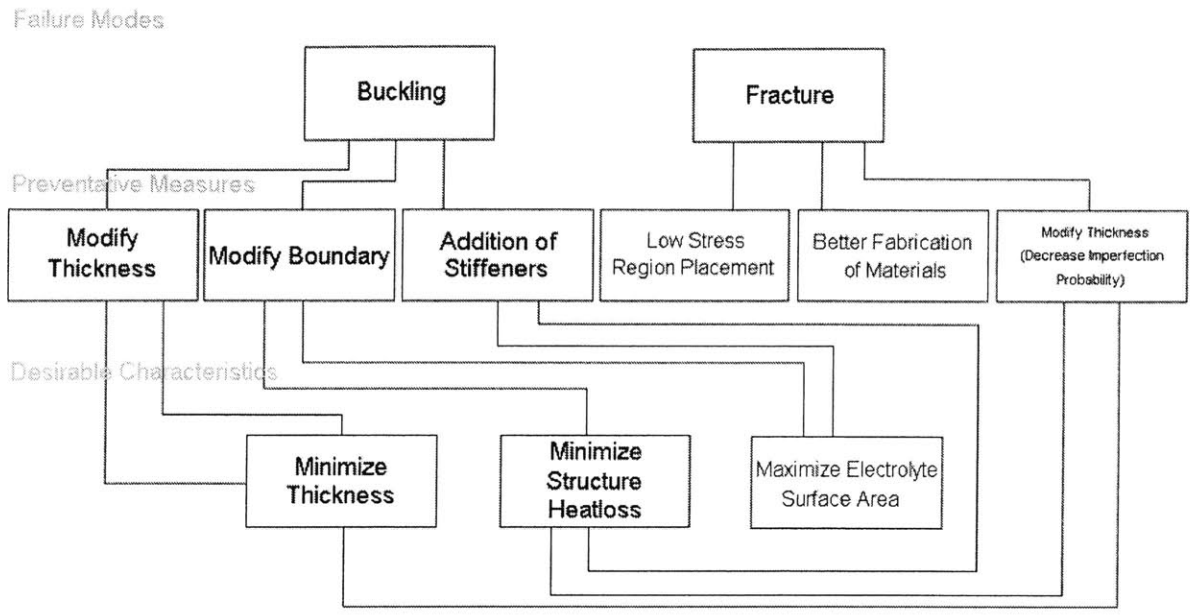

Figure 2-4: Failure Modes, their Preventative Measures, and their Impact on Design Variables

of the plate, and/or adding stiffeners to the plate. Yet increasing the thickness of the plate to avoid buckling would be in conflict with the design requirement of minimizing plate thickness, and minimizing heat loss (heat loss out of the plate boundary increases with thickness). Similarly, both decreasing the side length of the plate and adding stiffeners would go against the requirement of maximizing the YSZ surface area. Therefore the design of this plate structure is a balance between preventing structural failure, and at the same time fulfilling the design requirements as much as possible to maximize fuel cell power generation capability.

2.7 Required Analyses and Tools for Micro-Chemical SOFC Design

In order to obtain the correct balance between preventative measures and design requirements, tools must be developed to obtain an understanding of the mechanics, thermodynamics and the power generation of the fuel cell. Since the structural stability and power generation capability of the YSZ plate structure is crucial to the

operation of the fuel cell, a representative structure of a YSZ plate is analyzed.

The mechanics and failure of the representative YSZ structure is understood through the development of analytical models that describe the failure mechanisms of the plate, and the design variables that are involved. Equipped with these models, the design process can be streamlined by constructing a design map, indicating design spaces for which the structure would not fail. Furthermore, safe operating criteria for the representative structure can then be deduced, therefore aiding the design process.

Power generation of the plate structure is then understood through development of analytical thermodynamics models, following that of Chan *et al.* [24]. The heat loss and the power generation of a representative structure is analyzed. Coupled with the analytical models developed for the failure of fuel cell plate structures, net power generation of a fuel cell subject to maintaining structural stability can be assessed. Although the results give only an order of magnitude estimate on the power generation capability, it suffices for the purposes of providing an initial design estimate by which to compare candidate designs.

The four-step analysis procedure, namely safe operating criteria, heat loss, power generation and net power generation, will then be used all together to construct a design spreadsheet. Such a spreadsheet will serve the purpose of making the design process more efficient.

All the analyses and tools mentioned will be developed in the following chapters.

Chapter 3

Modeling of Micro-fabricated SOFC: Uniform Temperature Distribution

Having identified the generic configuration of a micro-fabricated SOFC, the specific dimensions and geometry of the membrane structure must be determined. To narrow down the scope of initial design analyses, only elliptical and rectangular plates are considered, where the criteria for selecting one geometry over another are its resistance to structural failure and its heat loss. To ensure a fair basis for comparison between these geometries, the in-plane surface areas are set equal at $40000\mu m^2$ for both geometries(since the in-plane lengths of the YSZ plates proposed by Baertsch are approximately $200\mu m$ [3, 13]). Furthermore, since the exposed in-plane surface area of the YSZ layer governs the power generation capability of the device, this basis for comparison has an additional advantage in that it allows the determination of a particular geometry that maximizes buckling temperature change for the same power generation capability. Plates of various thicknesses are also considered, but only results from the same thickness should be compared. Using buckling as the failure criterion for this analysis, the temperature change from the stress-free temperature for buckling of different geometries is found analytically. The following are expressions for the buckling temperature change of elliptical and rectangular plates [23]:

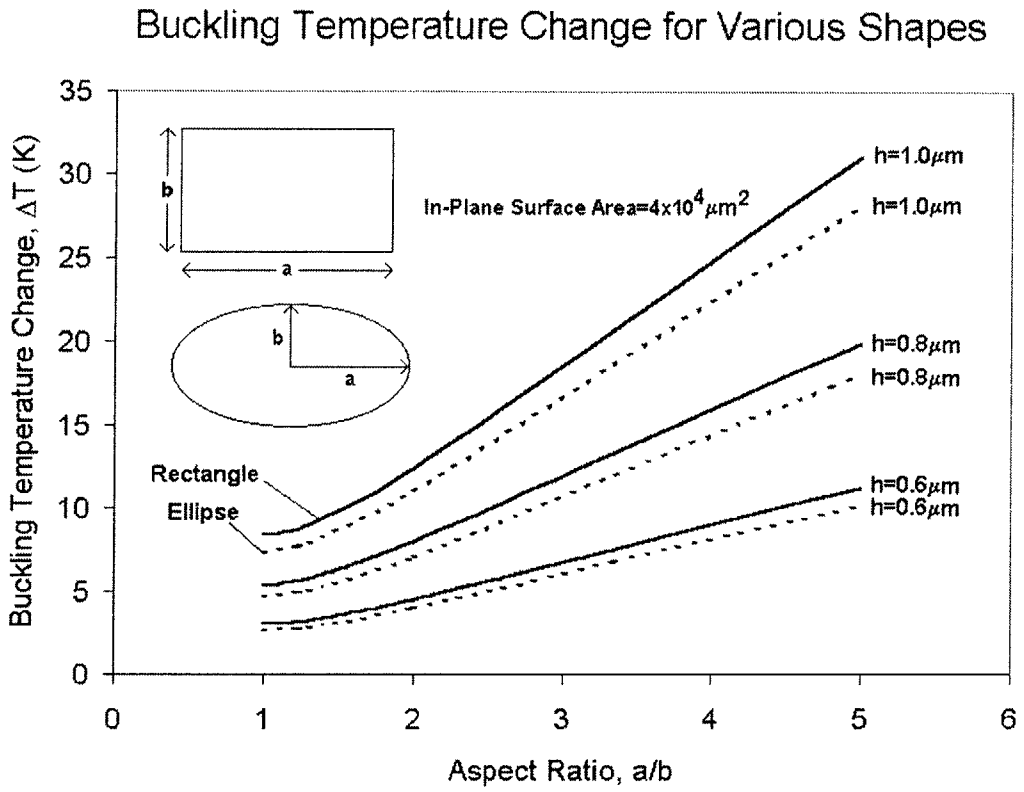

Figure 3-1: Buckling Temperature Change of Ellipses and Rectangles with Different In-Plane Aspect Ratios and Thicknesses

$$\Delta T = \frac{1.1t^2}{\alpha(1+\nu)}\left[\frac{3\gamma^4+2\gamma^2+3}{A\gamma(\gamma^2+1)}\right] \tag{3.1}$$

$$\Delta T = \Psi\left(\frac{a}{b}\right)\frac{\pi\gamma t^2}{A\alpha(1+\nu)} \tag{3.2}$$

where ΔT is the temperature change from the stress-free temperature, $\gamma = a/b$, Ψ are constants associated with (a/b) ratios (the aspect ratios of the elliptical plates) [23]. These expressions are plotted in Figure 3-1.

The material properties required within eqn 3.1 and eqn 3.2 are listed in Table 3.1 along with their references. The thermal conductivity of silicon required in subsequent analyses is also listed in this table.

Figure 3-1 shows that rectangular plates give the highest temperature change before buckling, therefore rectangular plates are considered for subsequent analyses.

Properties of YSZ	Values	References
Young's Modulus	157GPa	[1, 37]
Coefficient of Thermal Expansion	10 $\times 10^{-6}$ /K	[1, 37]
Poisson Ratio	0.313	[1, 37]
Heat Conductivity	6W/mK	[18, 38]
Residual Stress	-500MPa	[5, 21, 34]
Properties of Silicon	**Values**	**References**
Heat Conductivity	141W/mK	[38, 37]

Table 3.1: Material Properties of YSZ and Silicon for Analyses

Although ellipses give a lower temperature change before buckling, circles have the least perimeter for a given in-plane surface area, therefore leading to the least heat loss for a given surface area. Furthermore, circular geometries are easier to fabricate than elliptical geometries. Hence circular plates will also be considered.

The plates will initially be at room temperature, with a residual stress of σ_{res}. At operating conditions, their temperatures will be increased to a uniform temperature distribution of temperature T_{op}.

3.1 Rectangular Plates

The use of the four-step analysis procedure will now be illustrated.

3.1.1 Design Criteria Against Failure

Safe Operating Criterion: Buckling of Rectangular Plates

Referring again to Figure 1-1, the approximate in-plane dimensions of the representative YSZ plate structure in the current design by Baertsch [3, 13] are on the order of 200μm, and the thickness is on the order of 0.1-1μm, implying that the design falls within the thin plate mechanics category.

The rectangular plate structure will be idealized as a plate infinite in one dimension, with two sides rigidly clamped. This is shown in Figure 3-2.

Furthermore, for the time being the material will be considered to be a single

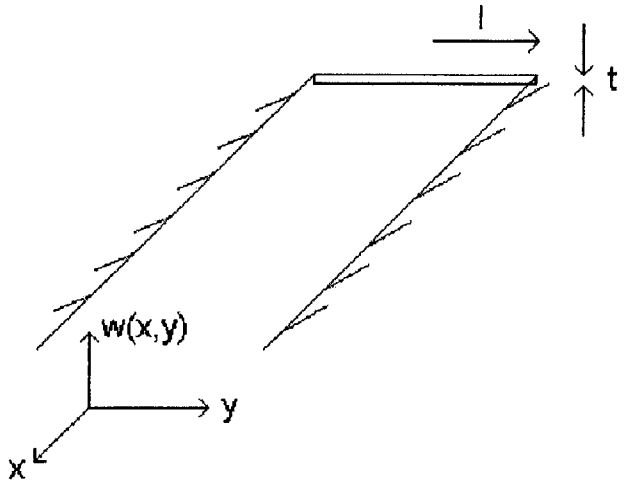

Figure 3-2: Idealized Clamped Rectangular Plate

isotropic material. Other assumptions are: 1) the deflection of the plate is small after buckling, 2) surfaces normal to the neutral surface prior to buckling are normal to the neutral surface after buckling 3) stresses perpendicular to the surface of the plate are approximately zero [36, 22].

Following Jensen [11], the assumed shape of the buckled plate is approximated as

$$w(x,y) = w_0\left(1 + cos\frac{\pi y}{l}\right)$$

where w_0 is an unknown displacement amplitude.

This yields a critical stress for buckling of

$$\sigma_{b,cr} = -\frac{E\pi^2 t^2}{12(1-\nu^2)l^2} \tag{3.3}$$

The in-plane stress of the YSZ plate, σ_p, is a sum of the residual stress measured at room temperature, and the thermally-induced stress resulting from the constrained expansion of the plate:

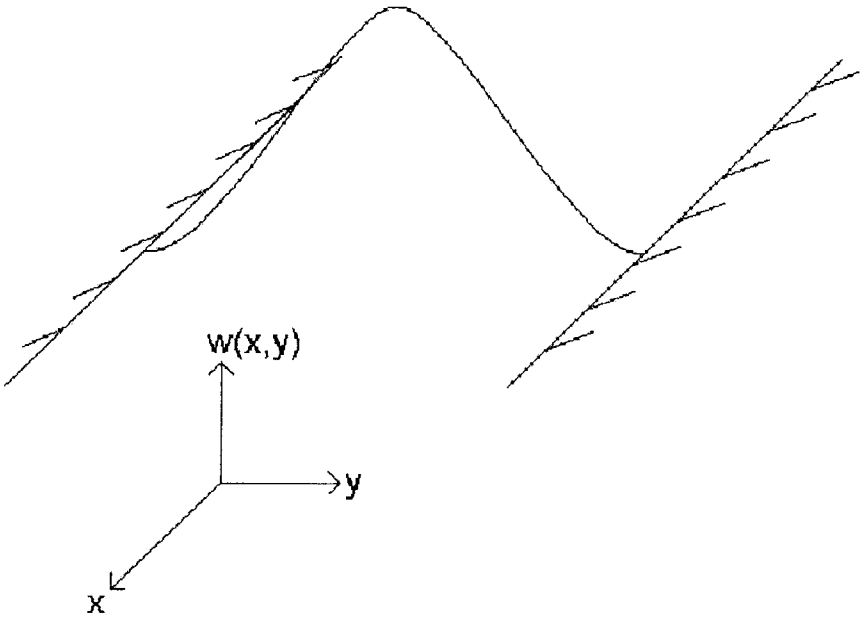

Figure 3-3: Assumed Buckled Shape of Infinite Plate

$$\sigma_p = \sigma_{res} + \sigma_{th} \tag{3.4}$$

The expression for σ_{th} is [36]

$$\sigma_{th} = -\frac{E\alpha\Delta T}{1-\nu} \tag{3.5}$$

Substituting eqn 3.5 into eqn 3.4 results in

$$\sigma_p = \sigma_{res} - \frac{E\alpha\Delta T}{1-\nu} \tag{3.6}$$

The critical condition for buckling is where $\sigma_p = \sigma_{b,cr}$. From a design point of view, the stress within the plate must never be close to the buckling stress. Therefore the maximum stress allowed in the plate should only be a fraction of the buckling stress. This is achieved by introducing a safety factor for buckling, S [22], defined to be

$$S = \frac{|\sigma_{b,cr}|}{|\sigma_p|} \tag{3.7}$$

where S assumes a value larger than 1 [27, 22].

Eliminating σ_p from eqn 3.6 using eqn 3.7 results in

$$\sigma_{res} - \frac{E\alpha\Delta T}{1-\nu} = -\frac{E\pi^2 t^2}{12S(1-\nu^2)l^2} \tag{3.8}$$

Rearranging the above equation, the following is the critical temperature change for buckling of a plate:

$$\Delta T_b = \frac{(1-\nu)}{E\alpha}\sigma_{res} + \frac{\pi^2}{12S\alpha(1+\nu)}\left(\frac{t}{l}\right)^2 \tag{3.9}$$

Therefore if

$$\Delta T_b > \frac{(1-\nu)}{E\alpha}\sigma_{res} + \frac{\pi^2}{12S\alpha(1+\nu)}\left(\frac{t}{l}\right)^2 \tag{3.10}$$

the safety limit is crossed, and the structure fails under safety factor considerations. By denoting $\zeta = t/l$, or the ratio of thickness to side length of the plate, 3.9 becomes:

$$\Delta T_b = \frac{(1-\nu)}{E\alpha}\sigma_{res} + \frac{\pi^2}{12S\alpha(1+\nu)}\zeta^2 \tag{3.11}$$

The introduction of the aspect ratio [27, 29] ζ will prove to be useful later when constructing the design map.

Safe Operating Criterion: Fracture of Rectangular Plates

The simplified structure in Figure 3-2 will again be used for consideration of failure by brittle fracture. Before proceeding with the analytical treatment, it is useful to first understand how fracture is treated mathematically in this thesis.

YSZ is a ceramic, and ceramics contain a stochastic distribution of flaws of different sizes throughout the material [15, 27]. Therefore for a ceramic material there is no deterministic fracture strength, and only a range for fracture strength can be provided [27]. Therefore it is more appropriate for the fracture strength to be understood as the probability of fracture for a specific loading condition.

The introduction of Weibull Statistics performed by Turner [35] is as follows:
The following expression is the probability of fracture [8]:

$$P_f(\sigma, V) = 1 - exp\left(-\frac{V}{V_0}\left[\left(\frac{\sigma_1}{\sigma_0}\right)^m + \left(\frac{\sigma_2}{\sigma_0}\right)^m + \left(\frac{\sigma_3}{\sigma_0}\right)^m\right]\right) \tag{3.12}$$

In the above equation, P_f is the probability of fracture failure, σ_1, σ_2, σ_3 are the three principal stresses of the plate, V_0 and σ_0 are the reference volume and stress of the experiment determining m, the Weibull Modulus.
Since the plate is infinite in the x-direction($\sigma_1 = 0$), and assuming that the plate is sufficiently thin($\sigma_3 \approx 0$) [22, 26], the following is the probability that the plate does *not* fail by fracture, denoted by P_s:

$$P_s = e^{-\frac{V}{V_0}\left(\frac{\sigma}{\sigma_0}\right)^m} \tag{3.13}$$

where $\sigma_2 = \sigma$.
Letting $\sigma = \sigma_p$ in eqn 3.13, and substituting the resulting expression into eqn 3.6, the allowable temperature change ensuring a probability of survival from fracture of P_s is

$$\Delta T_f = \frac{1-\nu}{E\alpha}\left[\sigma_{res} - \sigma_0\left(-\frac{V_0}{V} log P_s\right)^{\frac{1}{m}}\right] \tag{3.14}$$

Similar to the buckling criteria, if

$$\Delta T_f < \frac{1-\nu}{E\alpha}\left[\sigma_{res} - \sigma_0\left(-\frac{V_0}{V} log P_s\right)^{\frac{1}{m}}\right] \tag{3.15}$$

the structure is considered to have failed by fracture.

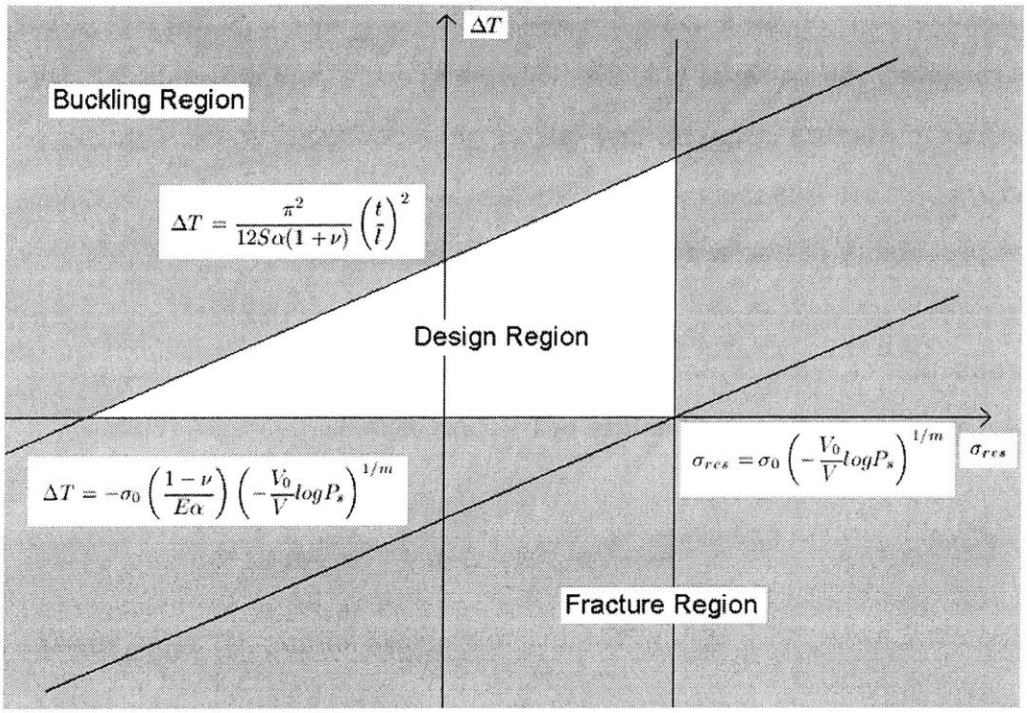

Figure 3-4: Design Map Showing Possible Design Region, Buckle Failure Region, and Fracture Failure Region

Inequalities eqn 3.10 and eqn 3.15 can be used to draw up a design map showing possible design regions. To do this, two variables need to be chosen as the axes of the design map. One factor for the choice of variables is that both failure modes considered, buckling and fracture, should be dependent on each of those variables. This would allow both failure modes to be placed on a single design map. Another factor should be that the choice of variable will allow the easier use of the design map [27]. With both these factors in mind and observing eqn 3.10 and eqn 3.15, a reasonable choice is to pick temperature change, ΔT, and residual stress, σ_{res}, as the two axes [27]. If ΔT is taken to be the y-axis and σ_{res} is taken to be the x-axis, a design map as shown in Figure 3-4 can be drawn using eqn 3.10 and eqn 3.15 .

Using suggestions from Turner [35, 33], more areas in Figure 3-4 are shaded away. To obtain the possible design region(the triangularly-shaped region in Figure 3-4), the following further steps were taken [35, 33]:

1. It was stated previously that the plate structure is assumed to be initially at

room temperature. This corresponds to the line $\Delta T = 0$. Since the plate structure is heated to make it operational, it must be the case that $\Delta T \geq 0$ under all circumstances. Therefore the region $\Delta T < 0$ is shaded off.

2. Since it was assumed that the device is at room temperature prior to its operation(when σ_{res} is measured), the initial state of the device on the design map must necessarily be on the line $\Delta T = 0$. Inspecting Figure 3-4, there are regions where at the initial state, the structure would already have been fractured. Therefore the region that should be shaded off is given by the inequality

$$\sigma_{res} \geq \sigma_0 \left(-\frac{V_0}{2V} log P_s \right)^{1/m} \tag{3.16}$$

Although fracture is assessed in this section, it will be disregarded in the rest of the thesis. The reasoning for this is as follows:
It is a fundamental design requirement that the plate structure be stable after it is fabricated. Therefore to allow for mechanics analyses for the plate structure in the first place, the plate structure must not have fractured initially. This assumption is made throughout the entire thesis. Furthermore, the plate is assumed to be at room temperature after fabrication, and that it is stable at that particular temperature. The structure then would only be subjected to a temperature increase to make it operational, since it was stated previously that $\Delta T \geq 0$ at all times. Since $\Delta T \geq 0$ and $\alpha_{YSZ} > \alpha_{Si}$ [22], the stresses within the structure could only become more compressive, thus rendering the only relevant failure mode to be buckling.

Although Figure 3-4 identifies design regions where designs are structurally stable, there is another approach that allows the convenient coupling between stability and power analyses, and gives way to the construction of a design spreadsheet, therefore streamlining the design process.
This approach can be understood by considering the following argument:
Eqn 3.8 is a design stability condition for the structure. Out of the three design variables t, l and ΔT, if two of these variables are chosen, then the third variable

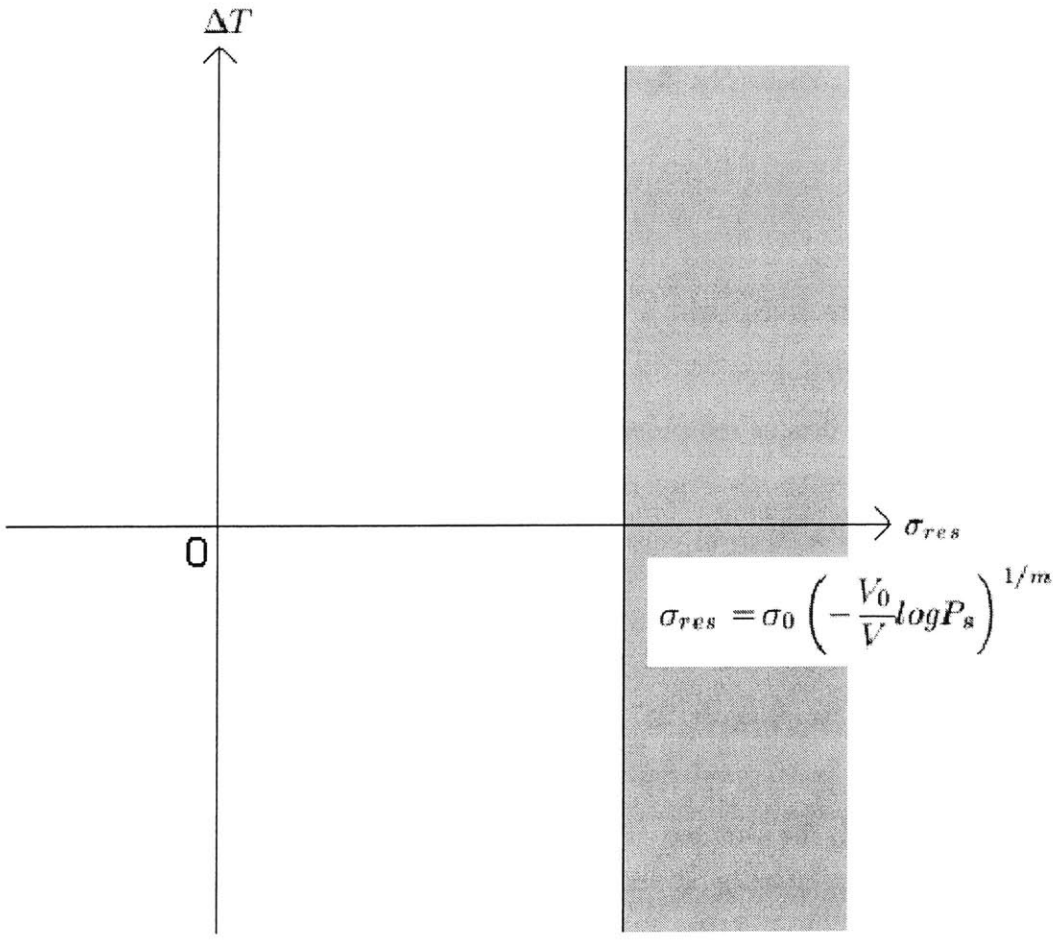

Figure 3-5: Region Shaded Away due to Fracture at Room Temperature

is determined, and this design possesses structural stability. Since the choice of t is limited to a small fabrication range of 0.1-1μm, t is chosen to be fixed. It is now possible to specify a range of ΔT $(= T_{op} - T_{room})$, and to find the corresponding maximum l that would ensure structural stability. Rearranging eqn 3.8,

$$l = \left\{ \frac{E\pi^2 t^2}{12S(1+\nu)[E\alpha\Delta T - \sigma_{res}(1-\nu)]} \right\}^{\frac{1}{2}} \tag{3.17}$$

One concern regarding the validity of eqn 3.17 is the situation where $E\alpha\Delta T - \sigma_{res}(1-\nu) < 0$. If this were the case, then

$$\begin{aligned} E\alpha\Delta T - \sigma_{res}(1-\nu) &< 0 \\ \frac{E\alpha\Delta T}{1-\nu} - \sigma_{res} &< 0 \\ -\frac{E\alpha\Delta T}{1-\nu} + \sigma_{res} &> 0 \end{aligned}$$

Noting that

$$\begin{aligned} \sigma_{th} &= -\frac{E\alpha\Delta T'}{1-\nu} \\ \sigma_p &= \sigma_{th} + \sigma_{res} \\ \Rightarrow \sigma_p &> 0 \end{aligned}$$

Therefore $E\alpha\Delta T - \sigma_{res}(1-\nu) < 0$ implies a tensile state of stress in the plate. Similarly $E\alpha\Delta T - \sigma_{res}(1-\nu) > 0$ means that the plate is in a state of compression. Since it is impossible for buckling to occur for in-plane tensile stresses, any l could be chosen and buckling will not occur.

Thus if the plate were under compressive stress$(E\alpha\Delta T - \sigma_{res}(1-\nu) > 0)$, the value for l is limited by eqn 3.17; if the plate were under tensile stress$(E\alpha\Delta T - \sigma_{res}(1-\nu) < 0)$, any l could be chosen (in relation to buckling only). These two conditions and eqn 3.17 will be applied to power analyses and the design spreadsheet to ensure structural

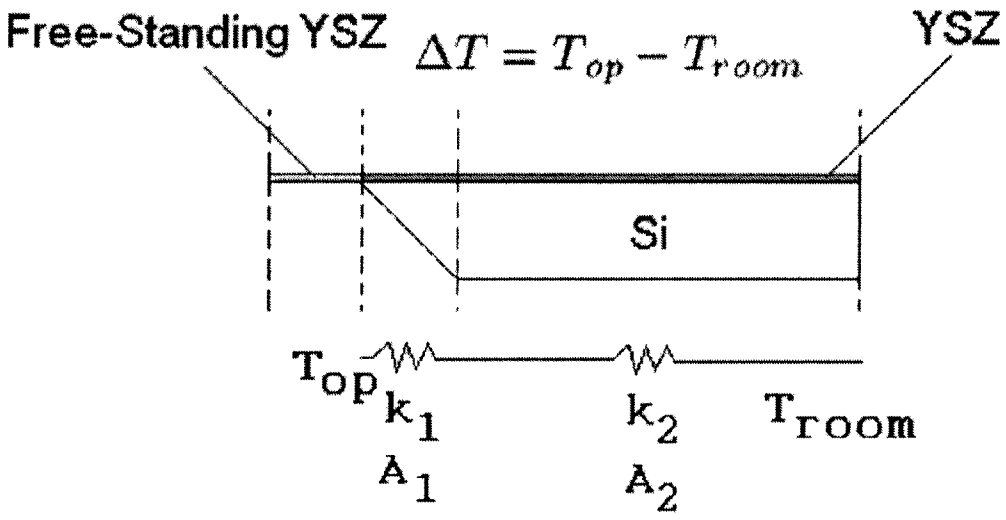

Figure 3-6: Schematic of Structure for Heat Loss Modeling

stability. Note that eqn 3.17 is the safe operating condition.

3.1.2 Heat Loss of Rectangular Plates

To find the net power generated by the plate structure, heat loss from the plate must be modeled. It is apparant that heat loss arises due to heat conduction out of the plate and heat convection from the plate to the fuel/oxygen flowing on either side of the plate structure. It will be assumed that the dominating mode of heat loss is conduction out of the sides of the plate; convection of heat from the plate to the fuel/oxygen will be ignored [35]. Figure 3-6 is a schematic of the structure modeled for heat loss.

Since the plate is infinite in the x-direction, heat loss is assumed to be one-dimensional in the y-direction. Figure 3-6 is then approximated by a two-resistor heat conduction system. The heat conductivity associated with each thermal resistor is calculated by averaging conductivities between the YSZ and the silicon regions, and the cross sectional area is the average between the area where heat enters and exits the resistor. Taking into account the 54.7^0 etch angle between the silicon and YSZ, and assuming that the thickness of the silicon is approximately 500μm [35], the averaged heat conductivities (in W/mK) and areas for each resistor are calculated to

be:

$$\begin{aligned} k_1 &= k_{YSZ}\frac{A_{YSZ}}{A_{YSZ}+A_{Si}} + k_{Si}\frac{A_{Si}}{A_{YSZ}+A_{Si}} \\ &= k_{YSZ}\frac{0.00071t}{0.00071t+(0.5)(0.00071)(0.0005)} + k_{Si}\frac{(0.5)(0.00071)(0.0005)}{0.00071t+(0.5)(0.00071)(0.0005)} \end{aligned}$$

$$k_2 = k_{YSZ}\frac{t}{0.0005+t} + k_{Si}\frac{0.0005}{0.0005+t} \tag{3.18}$$

Defining the length in the y-direction as β(where it will later be eliminated),

$$\begin{aligned} A_1 &= \frac{t\beta+(t+0.0005)\beta}{2} \\ \frac{A_1}{\beta} &= \frac{1}{2}(2t+0.0005) \end{aligned}$$

$$\begin{aligned} A_2 &= (0.0005+t)\beta \\ \frac{A_2}{\beta} &= 0.0005+t \end{aligned}$$

Assuming that the outermost boundary of the silicon is at room temperature, the heat loss (in W) from the plate is

$$\begin{aligned} Q &= \frac{2(T_B-T_{room})}{\frac{0.00071}{\beta(k_1A_1/\beta)}+\frac{L-l-0.00071}{\beta(k_2A_2/\beta)}} \\ &= \frac{2\Delta T_B}{\frac{0.00071}{\beta(k_1A_1/\beta)}+\frac{L-l-0.00071}{\beta(k_2A_2/\beta)}} \end{aligned}$$

$$q = \frac{Q}{2\beta l} = \frac{\Delta T_B}{l\left(\frac{0.00071}{k_1A_1/\beta}+\frac{L-l-0.00071}{k_2A_2/\beta}\right)}$$

$$\Rightarrow q = \frac{\Delta T_B}{l\left[\frac{0.00142}{k_1(2t+0.0005)} + \frac{L-l-0.00071}{k_2(0.0005+t)}\right]} \tag{3.19}$$

where L is half the side length of the silicon die(assumed to be 5mm [27]), l is half the width of the free-standing YSZ plate, and q is the heat loss per unit plate area (in W/m^2).

3.1.3 Power Generation of Plate Structure

The power per unit area of an SOFC YSZ plate structure is given by the following expression [24, 37, 39, 10]:

$$p = i(E_0 - \eta_{ohm} - \eta_{act,a} - \eta_{act,c}) \tag{3.20}$$

where

$$\begin{aligned}
E_0 &= \frac{R_g T_{op}}{2F} logK_p - \frac{R_g T_{op}}{4F} log\left(\frac{\rho_{H_2O}^2 \rho_0}{\rho_{H_2}^2 \rho_{O_2}}\right) \quad \text{Open Circuit Potential} \\
\eta_{ohm} &= \frac{it}{\sigma_e} = it10^{4.27\left(\frac{1000}{T_{op}}\right)-4.41} \quad \text{Ohmic Potential} \\
\eta_{act,a} &= \frac{2R_g T_{op}}{F} arcsinh\left(\frac{i}{4i_0}\right) \quad \text{Anode Activation Potential} \\
\eta_{act,c} &= \frac{2R_g T_{op}}{F} arcsinh\left(\frac{i}{2i_0}\right) \quad \text{Cathode Activation Potential}
\end{aligned}$$

Definitions of the symbols in the above list of equations are listed in Appendix A, and the expression for $1/\sigma_e$ is approximated from the data presented in [30].
The partial pressures for the reaction concerned can be obtained from the following equation:

$$H_2 + \frac{1}{2}O_2 \leftrightharpoons H_2O$$

Therefore $\rho_{H_2} = 1$, $\rho_{O_2} = 1/2$, $\rho_{H_2O} = 1$, and the reference pressure $\rho_0 = 1$. Furthermore, the logarithm of the reaction equilibrium constant $logK_p$ can be found

from [39], and the following equation approximates the data to a good degree of accuracy:

$$logK_p = 129025T_{op}^{-1.2596} \tag{3.21}$$

Knowing that $T_{op} = \Delta T + T_{room}$, therefore

$$\begin{aligned} p = \frac{iR_g(\Delta T + T_{room})}{2F}[129025(\Delta T + T_{room})^{-1.2596}] \\ - \frac{iR_g(\Delta T + T_{room})}{4F}log2 \\ - i^2t10^{4.27(\frac{1000}{\Delta T + T_{room}})-4.41} \\ - \frac{2iR_g(\Delta T + T_{room})}{F}\psi(i) \end{aligned} \tag{3.22}$$

where

$$\psi(i) = arcsinh\left(\frac{i}{4i_0}\right) + arcsinh\left(\frac{i}{2i_0}\right)$$

Since the temperature distribution of the plate is uniform, every point on the plate has the same value for p.

One additional issue that surfaces is the current that should run through the circuit that generates the maximum power. Assuming that there are mechanisms adjusting the current to maximize power generation, for different operating conditions and different SOFC designs there is a particular current that maximizes power generation. This current can be found through the following expression, and solving for i:

$$\frac{\partial p}{\partial i} = 0 \tag{3.23}$$

The resulting equation to be solved is a transcendental equation. i can then be found by the "bisection method" [7].

In subsequent calculations for power generated of an SOFC, only the maximum power is presented.

3.1.4 Net Power Generation of a Structurally Stable Rectangular Plate

The net power generation of a plate structure is then simply the power per unit area minus the heat loss per unit area, or

$$p_{net} = p - q \tag{3.24}$$

p_{net} is coupled with the safe operating condition by specifying that t, ΔT and l in eqn 3.17 be the same as those in expression for p_{net}. This means that p_{net} calculated are those for stable plates.

3.2 Circular Plates

The analyses for circular plates are similar to those for rectangular plates. The four-step analysis procedure is again carried out.

3.2.1 Safe Operating Criterion: Buckling of Circular Plates

The circular plate modeled in this section is shown in Figure 3-7.

The buckling stress for such a circular plate is [23]

$$\sigma_{b,cr} = -1.22\frac{E}{1-\nu^2}\left(\frac{t}{R}\right)^2 \tag{3.25}$$

Using eqn 3.6 and eqn 3.7, the largest circular plate radius R with a stress safety factor S for a particular t and ΔT is

$$R = \left\{\frac{1.22Et^2}{S(1+\nu)[E\alpha\Delta T - \sigma_{res}(1-\nu)]}\right\}^{1/2} \tag{3.26}$$

3.2.2 Heat Loss of Circular Plates

The schematic of the plate modeled for heat loss is shown in Figure 3-8.

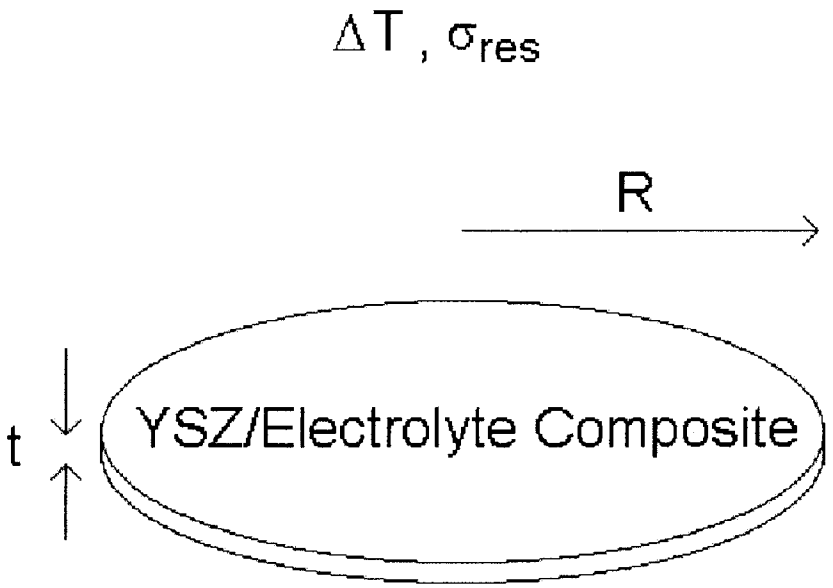

Figure 3-7: Schematic of Circular Plate Modeled

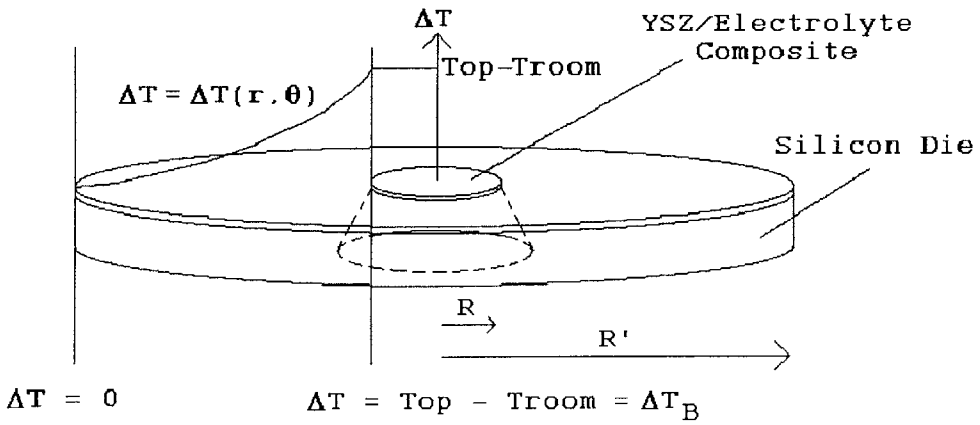

Figure 3-8: Schematic of Circular Plate Heat Loss Modeling

Modeling the heat loss as two-dimensional steady state conduction, Laplace Equation then holds:

$$\frac{\partial^2 \Delta T}{\partial r^2} + \frac{1}{r}\frac{\partial \Delta T}{\partial r} + \frac{1}{r^2}\frac{\partial^2 \Delta T}{\partial \theta^2} = 0 \tag{3.27}$$

Assuming that $\Delta T(r,\theta) = \Gamma(r)\Theta(\theta)$ [32], the solution is [32]:

$$\Delta T(r,\theta) = \frac{1}{2}(C_0 + D_0 log r) + \Sigma_{n=1}^{\infty}\left[\left(C_n r^n + \frac{D_n}{r^n}\right)cos(n\theta) + \left(A_n r^n + \frac{B_n}{r^n}\right)sin(n\theta)\right] \tag{3.28}$$

The constants C_0, D_0, A_n, B_n, C_n and D_n are found through the following boundary conditions [32]:

$$\begin{aligned} \Delta T(R,\theta) &= \Delta T_B \\ \Delta T(R',\theta) &= 0 \end{aligned}$$

The temperature difference distribution is then

$$\Delta T(r) = \frac{\Delta T_B}{log(R'/R)} log\left(\frac{R'}{r}\right) \tag{3.29}$$

The total power loss out of this structure is

$$Q = -kA\left.\frac{\partial \Delta T}{\partial r}\right|_{r=R} \tag{3.30}$$

In order to use eqn 3.30, k and A must be found. Considering the structure outside the free-standing YSZ plate, average values of k and A are found through the following process:

The volume of YSZ outside the free-standing plate is simply $V_{YSZ} = (\pi R'^2 - \pi R^2)t$. However, to find the volume of silicon, it is first separated into two portions, finding the volume of each and finally summing them together. The two portions are shown in Figure 3-9.

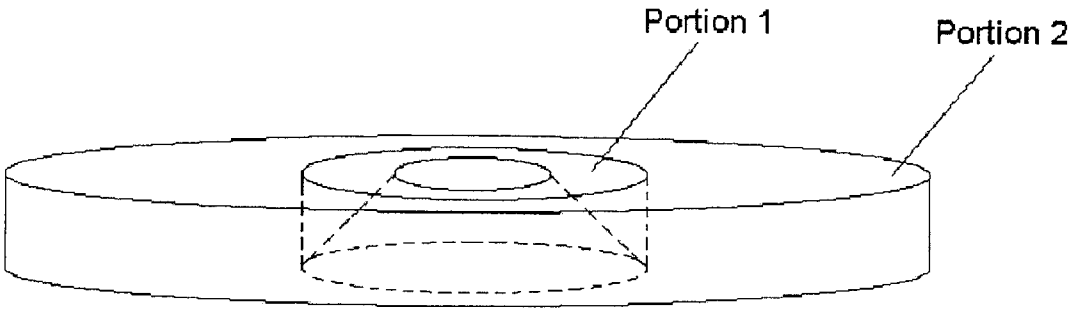

Figure 3-9: Two Portions for Consideration of the Volume of Silicon

The volume of the second portion is $(\pi R'^2 - \pi(0.00071)^2)(0.0005)$. As for the first portion, the volume is found by integrating the expression for a cone with the limits shown:

The expression for the cone shown is [31]

$$z = \left(\frac{x^2+y^2}{(tan54.7^0)^2}\right)^{1/2} - \frac{R}{tan54.7^0} \tag{3.31}$$

Although the use of an anisotropic wet etch will not result in a conical surface, nevertheless it is a useful approximation for modeling purposes.
The volume is then

$$\begin{aligned} \text{Volume} &= \int_0^{2\pi}\int_R^{0.00071} z dx dy \\ &= \int_0^{2\pi}\int_R^{0.00071} \frac{1}{tan54.7^0}(r-R) r dr d\theta \\ &= \frac{2\pi}{tan54.7^0}\left[\frac{1}{3}(0.00071)^3 - \frac{R}{2}(0.00071)^2 + \frac{1}{6}R^3\right] \end{aligned}$$

The total volume of silicon, V_{Si}, is then

$$V_{Si} = \frac{\pi}{3(tan54.7^0)}[2(0.00071)^3 - 3R(0.00071)^2 + R^3] + \pi[R'^2 - (0.00071)^2](0.0005) \tag{3.32}$$

The value of k is then

$$k = k_{YSZ}\frac{V_{YSZ}}{V_{Si}+V_{YSZ}} + k_{Si}\frac{V_{Si}}{V_{Si}+V_{YSZ}} \tag{3.33}$$

The averaged area is

$$A = \pi[R't + R'(t + 0.0005)] \tag{3.34}$$

The heat loss during steady state operation can then be found from the following equation [16]:

$$\begin{aligned} Q &= -kA\left.\frac{\partial \Delta T}{\partial r}\right|_{r=R} \\ &= \frac{kA\Delta T_B}{Rlog(R'/R)} \end{aligned}$$

The heat loss per unit area of the free-standing YSZ plate is then

$$q = \frac{kA\Delta T_B}{\pi R^3 log(R'/R)} \tag{3.35}$$

3.2.3 Power Generation of Circular Plates

Since the circular plate is exposed to a uniform temperature distribution, the power per unit area for a circle is also given by eqn 3.22.

3.2.4 Net Power Generation of Structurally Stable Circular Plates

Similar to rectangular plates, the net power generation p_{net} is also given by eqn 3.24. The coupling between the net power and the safe operating condition is again achieved by applying both equations assuming the same R, t and ΔT.

Maximum Temperature of Temperature Profile (K)	Maximum Temperature Difference from Room Temperature of Temperature Profile (K)	Tensile=0, Compressive=1 at Operation	Does Maximum Radius Exist, If yes, Radius of Plate with Safety Factor (m)	q (W/m^2)	Ideal Current (A/m^2)	p (W/m^2)	p_{net}(W/m^2)
293	0	1	1.8812364497E-06	0.0000E+00	0.000434992	2.7564E-04	2.7564E-04
323	30	1	1.7641708264E-06	3.4187E+07	0.009568839	5.9093E-03	-3.4187E+07
373	80	1	1.6098078432E-06	1.0824E+08	0.544922054	3.2393E-01	-1.0824E+08
423	130	1	1.4899614629E-06	2.0337E+08	11.84723377	6.8108E+00	-2.0337E+08
473	180	1	1.3934291885E-06	3.1932E+08	129.2304993	7.2097E+01	-3.1932E+08
523	230	1	1.3135162079E-06	4.5589E+08	746.8170166	3.9761E+02	-4.5589E+08
573	280	1	1.2459429111E-06	6.1290E+08	2498.178482	1.1400E+03	-6.1290E+08
593	300	1	1.2216905405E-06	6.8139E+08	3600.451279	1.5043E+03	-6.8139E+08
613	320	1	1.1988014042E-06	7.5312E+08	4862.223434	1.8515E+03	-7.5312E+08
633	340	1	1.1771523956E-06	8.2809E+08	6143.402863	2.1361E+03	-8.2809E+08
653	360	1	1.1566354300E-06	9.0627E+08	7256.22406	2.3226E+03	-9.0627E+08
673	380	1	1.1371551672E-06	9.8767E+08	8023.926544	2.3970E+03	-9.8767E+08
693	400	1	1.1186271428E-06	1.0723E+09	8352.960205	2.3708E+03	-1.0723E+09
713	420	1	1.1009762227E-06	1.1601E+09	8268.527985	2.2724E+03	-1.1601E+09
733	440	1	1.0841353190E-06	1.2511E+09	7884.268951	2.1335E+03	-1.2511E+09
753	460	1	1.0680443147E-06	1.3453E+09	7335.299683	1.9798E+03	-1.3453E+09
773	480	1	1.0526491593E-06	1.4427E+09	6729.0802	1.8273E+03	-1.4427E+09
788	495	1	1.0415299375E-06	1.5178E+09	6278.130341	1.7189E+03	-1.5178E+09
803	510	1	1.0307557918E-06	1.5947E+09	5848.144531	1.6175E+03	-1.5947E+09
818	525	1	1.0203092349E-06	1.6734E+09	5446.750641	1.5237E+03	-1.6734E+09
833	540	1	1.0101739958E-06	1.7538E+09	5077.004242	1.4373E+03	-1.7538E+09
848	555	1	1.0003349129E-06	1.8361E+09	4739.025879	1.3582E+03	-1.8361E+09
863	570	1	9.9077783847E-07	1.9201E+09	4431.438446	1.2856E+03	-1.9201E+09
878	585	1	9.8148955338E-07	2.0059E+09	4152.095032	1.2192E+03	-2.0058E+09
893	600	1	9.7245769000E-07	2.0934E+09	3898.542023	1.1582E+03	-2.0934E+09
908	615	1	9.6367066298E-07	2.1827E+09	3668.299103	1.1023E+03	-2.1827E+09
923	630	1	9.5511760682E-07	2.2738E+09	3459.011078	1.0508E+03	-2.2738E+09
938	645	1	9.4678831931E-07	2.3667E+09	3268.453217	1.0033E+03	-2.3667E+09

Table 3.2: Design Spreadsheet for Circular Plates under Uniform Temperature Distribution

With the four-step analysis procedure performed for both plate geometries, a comparison between rectangular and circular plates is now possible.

3.3 Comparison between Rectangular and Circular Plates

Using the non-buckling conditions, expressions for heat loss per unit area, power generated per unit area and the net power generated per unit area, design spreadsheets are constructed for uniform temperature distributions over circular and rectangular plates. These are presented in Table 3.2 and Table 3.3. These design spreadsheets are then in turn used to assess the power generation and heat loss under uniform temperature distribution for both plate geometries.

Instead of presenting a single graph and plotting p_{net} with operation temperature T_{op} directly, separate graphs for power generation and heat loss are plotted for clarity. Figure 3-10 shows that the power per unit area of a rectangle superimposes on that

Maximum Temperature of Temperature Profile (K)	Maximum Temperature Difference from Room Temperature of Temperature Profile (K)	Tensile=0, Compressive=1 at Operation	Does Maximum Side Length Exist, if yes, 0.5*Side Length of Plate with Safety Factor, or "I"(m)	q (W/m^2)	Ideal Current (A/m^2)	p (W/m^2)	p_{net}(W/m^2)
293	0	1	1.5446237687E-06	0.0000E+00	0.000434992	2.7564E-04	2.7564E-04
323	30	1	1.4485049055E-06	2.5578E+08	0.00956884	5.9093E-03	-2.5578E+08
373	80	1	1.3217623389E-06	7.4747E+08	0.544922407	3.2393E-01	-7.4747E+08
423	130	1	1.2233602640E-06	1.3123E+09	11.84722959	6.8108E+00	-1.3123E+09
473	180	1	1.1441006647E-06	1.9429E+09	129.2305089	7.2097E+01	-1.9429E+09
523	230	1	1.0784666421E-06	2.6336E+09	746.8168234	3.9761E+02	-2.6336E+09
573	280	1	1.0230043439E-06	3.3800E+09	2498.175924	1.1400E+03	-3.3800E+09
593	300	1	1.0030914889E-06	3.6933E+09	3800.449092	1.5043E+03	-3.6933E+09
613	320	1	9.8429794258E-07	4.0147E+09	4862.21891	1.8515E+03	-4.0147E+09
633	340	1	9.6852262587E-07	4.3440E+09	6143.407898	2.1361E+03	-4.3440E+09
653	360	1	9.4967679384E-07	4.6812E+09	7256.217782	2.3226E+03	-4.6811E+09
673	380	1	9.3368216582E-07	5.0258E+09	8023.929641	2.3970E+03	-5.0258E+09
693	400	1	9.1846939057E-07	5.3780E+09	8352.951068	2.3708E+03	-5.3780E+09
713	420	1	9.0397677800E-07	5.7374E+09	8268.55252	2.2724E+03	-5.7374E+09
733	440	1	8.9014924427E-07	6.1040E+09	7884.283924	2.1335E+03	-6.1040E+09
753	460	1	8.7693742922E-07	6.4775E+09	7335.309434	1.9798E+03	-6.4775E+09
773	480	1	8.6429695368E-07	6.8580E+09	6729.099737	1.8273E+03	-6.8580E+09
788	495	1	8.5516731214E-07	7.1478E+09	6278.148192	1.7189E+03	-7.1478E+09
803	510	1	8.4632100158E-07	7.4414E+09	5848.126635	1.6175E+03	-7.4414E+09
818	525	1	8.3774366391E-07	7.7387E+09	5446.753584	1.5237E+03	-7.7387E+09
833	540	1	8.2942193944E-07	8.0396E+09	5077.003078	1.4373E+03	-8.0396E+09
848	555	1	8.2134337944E-07	8.3442E+09	4739.031869	1.3582E+03	-8.3442E+09
863	570	1	8.1349636771E-07	8.6524E+09	4431.448936	1.2856E+03	-8.6524E+09
878	585	1	8.0587005040E-07	8.9641E+09	4152.102775	1.2192E+03	-8.9641E+09
893	600	1	7.9845427285E-07	9.2793E+09	3898.547271	1.1582E+03	-9.2793E+09
908	615	1	7.9123952270E-07	9.5980E+09	3668.30495	1.1023E+03	-9.5980E+09
923	630	1	7.8421687862E-07	9.9201E+09	3459.007134	1.0508E+03	-9.9201E+09
938	645	1	7.7737796390E-07	1.0246E+10	3268.461433	1.0033E+03	-1.0246E+10

Table 3.3: Design Spreadsheet for Rectangular Plates under Uniform Temperature Distribution

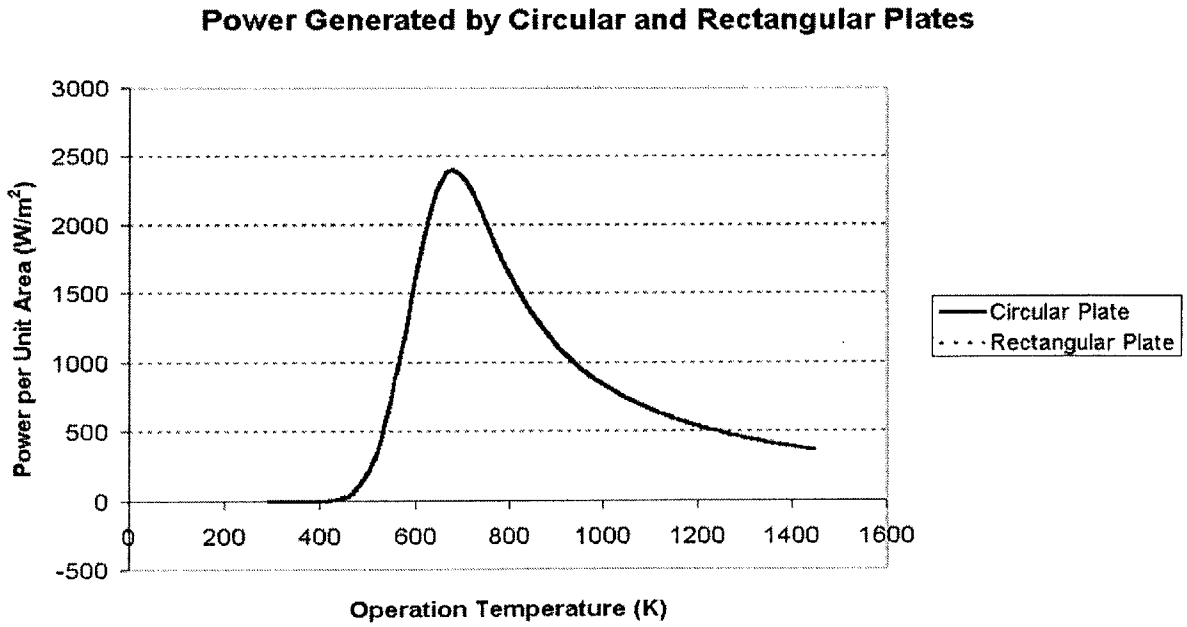

Figure 3-10: Power Generated per Unit Area by Stable Rectangular and Circular Plates

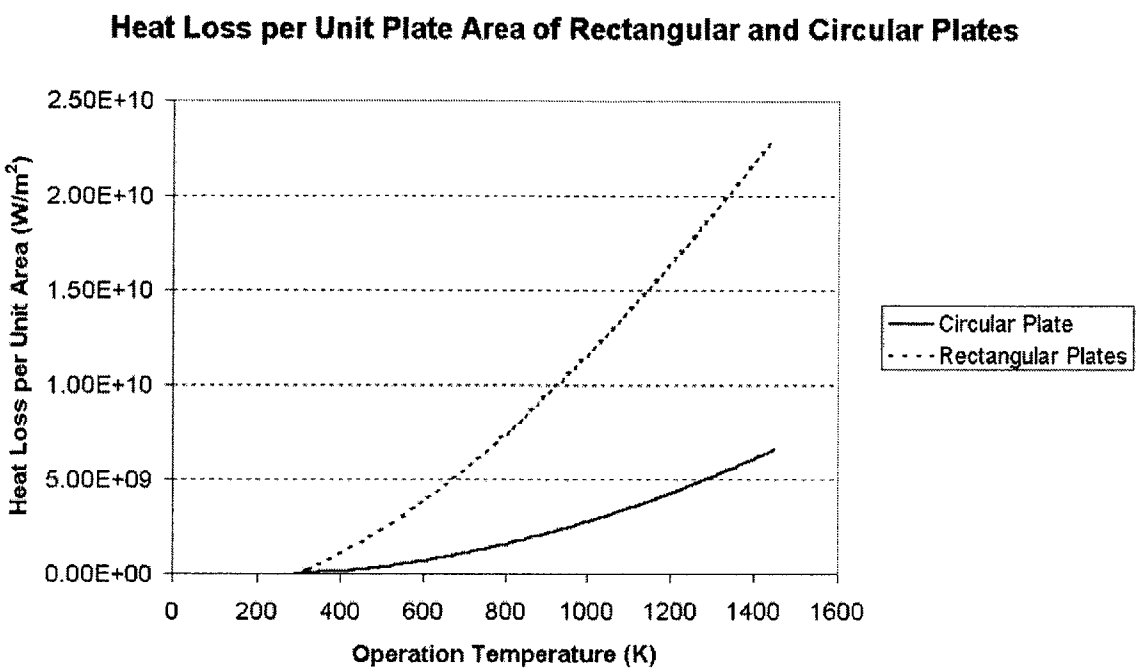

Figure 3-11: Heat Loss per Unit Area of Stable Rectangular and Circular Plates

of a circle. This is true because power per unit area is independent of geometry. Furthermore there is an optimal temperature for maximum power generation. Therefore for a uniform temperature distribution, that plate should be operating at that particular temperature. To confirm that the values obtained for power per unit area are in fact correct, the maximum value for power generation per unit area in this analysis is compared to that of a commercially available SOFC [25, 12], and they are in agreement within an order of magnitude.

Heat loss per unit area of stable plates are shown in Figure 3-11, and it shows that the amount of heat loss is detrimental to power generation. For example, for the temperature where there is maximum power generation for a rectangular plate, the heat loss is approximately 10^6 times larger than the power generated. The figure also shows that choosing a circle instead of rectangle for the plate geometry reduces heat loss. This is correct because for a given in-plane surface area, circles have the least perimeter, thus restricting heat loss.

Although a comparison between rectangular and circular plates has been achieved,

both plate structures failed to achieve the aim of producing a positive net power. One possible way to decrease this heat loss would be to lower the boundary temperature in eqn 3.35. However, if the temperature profile were uniform, decreasing the boundary temperature will also decrease the operation temperature, therefore lowering the power per unit area. Therefore non-uniform temperature profiles of the form where the temperature at the center of the plate is higher than that at the boundary should be considered.

Chapter 4

Modeling of Micro-fabricated SOFC: Non-Uniform Temperature Distribution

In this chapter non-uniform temperature distributions will be investigated in an attempt to decrease the conductive heat loss out of the plates. The power generation capability of rectangular and circular plates will again be found under such temperature distributions.

4.1 Normal Temperature Distribution

The first non-uniform temperature distribution investigated is the normal temperature distribution. This particular distribution is chosen because it has a simple functional form, along with specifiable temperature maxima location and temperature decay rate. Although it is true that specifying a particular temperature distribution initially may not be achievable in practice, the analyses performed for this temperature distribution will nevertheless provide insights into the effects of non-uniform temperature distributions and also need to develop analysis tools for dealing with non-uniform temperature distributions.

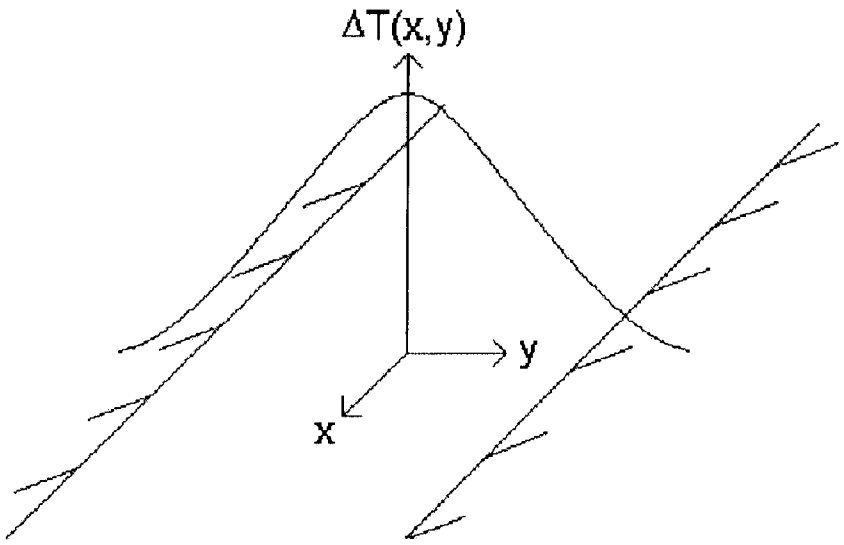

Figure 4-1: Normal Temperature Distribution over a Rectangular Plate (idealized to be infinite in the x-direction)

4.1.1 Rectangular Plates

Rectangular plates will again be approximated by a plate infinite in the x-direction. The normal temperature distribution across the rectangular plate is given by the following expression:

$$\Delta T(x,y) = \Delta T_m e^{-y^2/s^2} \tag{4.1}$$

The temperature distribution over the plate is shown in Figure 4-1.

Safe Operating Criterion: Buckling of Rectangular Plates

To determine the thermal stress resulting from the constrained expansion of the plate [35, 36], the deformation from the temperature distribution is first calculated, and through Hooke's Law, the thermal stress is then determined [27].
With $\Lambda = l/s$, the deformation δ resulting from the normal temperature distribution is

$$
\begin{aligned}
\delta &= \int_0^l \epsilon_{yy} dy \\
&= \int_0^l \alpha \Delta T_m e^{-y^2/s^2} dy \\
&= \frac{\alpha \Delta T_m s \sqrt{\pi}}{2} erf(l/s) \\
\Rightarrow \delta &= \frac{\alpha \Delta T_m s \sqrt{\pi}}{2} erf(\Lambda)
\end{aligned}
$$

Using Hooke's Law, the stress from the normal temperature distribution is [19, 26]

$$
\begin{aligned}
\sigma_{th} &= -\sigma_{yy} \\
&= -\frac{E}{1-\nu}\frac{\delta}{l} \\
&= -\frac{E\alpha \Delta T_m}{1-\nu}\frac{s}{l}\frac{\sqrt{\pi}}{2} erf(l/s) \\
\Rightarrow \sigma_{th} &= -\frac{E\alpha \Delta T_m \sqrt{\pi}}{2(1-\nu)\Lambda} erf(\Lambda)
\end{aligned}
$$

Again using eqn 3.6, eqn 3.7 and eqn 3.3, the maximum l that ensures safe operation is:

$$
\begin{aligned}
\sigma_{res} - \frac{E\alpha \Delta T_m \sqrt{\pi} erf(\Lambda)}{2\Lambda(1-\nu)} &= -\frac{E\pi^2 t^2}{12 S(1-\nu^2) l^2} \\
\Rightarrow l &= \left\{ \frac{E\pi^2 \Lambda t^2}{6S(1+\nu)[E\alpha \Delta T_m \sqrt{\pi} erf(\Lambda) - 2\Lambda(1-\nu)\sigma_{res}]} \right\}^{1/2}
\end{aligned}
$$

The dimensionless variable Λ is intepreted as the decay rate of the normal temperature distribution. It is one of the variables that defines the normal temperature distribution, and is used in lieu of s to simplify calculations.

Heat Loss of Rectangular Plates

Eqn 3.19 is also used here to describe the heat loss per unit area. However, the boundary temperature ΔT_B is now given by

$$\Delta T_B = \Delta T_m e^{-\Lambda^2} \tag{4.2}$$

Power Generation of Rectangular Plates

Unlike the previous chapter for uniform temperature distribution where power per unit area is the same at all points of the plates, the normal temperature distribution across the rectangular plate means that power per unit area is different at different locations on the plate. Therefore a single value for power per unit area is required for the normal temperature distribution in order to compare with the power per unit area for the uniform temperature distribution. An average power per unit area for a non-uniform temperature distribution is defined as

$$p_{ave} = \frac{1}{l}\int_0^l p(\Delta T)dy \tag{4.3}$$

Using eqn 3.22, p_{ave} is

$$\begin{aligned} p_{ave} = \frac{129025 i R_g}{2F}\frac{1}{l}\int_0^l (\Delta T_m e^{-y^2/s^2} + T_{room})^{-0.2596} dy \\ - \frac{i R_g log2}{4F}\left[\frac{1}{l}\int_0^l (\Delta T_m e^{y^2/s^2})dy + T_{room}\right] \\ - i^2 t \frac{1}{l}\int_0^l 10^{4.27\left(\frac{1000}{\Delta T_m e^{y^2/s^2}+T_{room}}\right)-4.41} dy \\ - \frac{2 i R_g}{F}\left[\frac{1}{l}\int_0^l \Delta T_m e^{-y^2/s^2} dy + T_{room}\right]\psi(i) \end{aligned} \tag{4.4}$$

Therefore

$$p_{ave} = \frac{129025iR_g}{2F}\frac{1}{\Lambda}\int_0^{\Lambda}(\Delta T_m e^{-\zeta^2} + T_{room})^{-0.2596}d\zeta$$
$$- \frac{iR_g log2}{4F}\left[\frac{\Delta T_m}{2\Lambda}erf(\Lambda) + T_{room}\right]$$
$$- i^2 t\frac{1}{\Lambda}\int_0^{\Lambda} 10^{4.27\left(\frac{1000}{\Delta T_m e^{-\zeta^2}+T_{room}}\right)-4.41}d\zeta$$
$$- \frac{2iR_g}{F}\left[\frac{\Delta T_m\sqrt{\pi}}{2\Lambda}erf(\Lambda) + T_{room}\right]\psi(i) \quad (4.5)$$

The integrals presented in the previous expression are computed by numerical means and using the definition of the Riemann Sum [28].

Since the present power under consideration is the average power p_{ave}, the current that should run through the circuit to maximize power generation is found by the following expression:

$$\frac{\partial p_{ave}}{\partial i} = 0 \quad (4.6)$$

Similar to Chapter 3, i is found through the "bisection method" [7].

The p_{ave} for stable structures is found by eqn 4.5 assuming the same ΔT, t and Λ as those in eqn 4.2.

Net Power Generation of Structurally Stable Rectangular Plates

The net power generation p_{net} is given by eqn 3.24, with p replaced by p_{ave}.

4.1.2 Circular Plates

The normal temperature distribution over a circular plate is assumed to be of the form

$$\Delta T(x,y) = \Delta T_m e^{-\frac{x^2+y^2}{s^2}} = \Delta T_m e^{-r^2/s^2} = \Delta T(r) \quad (4.7)$$

This is shown in Figure 4-2.

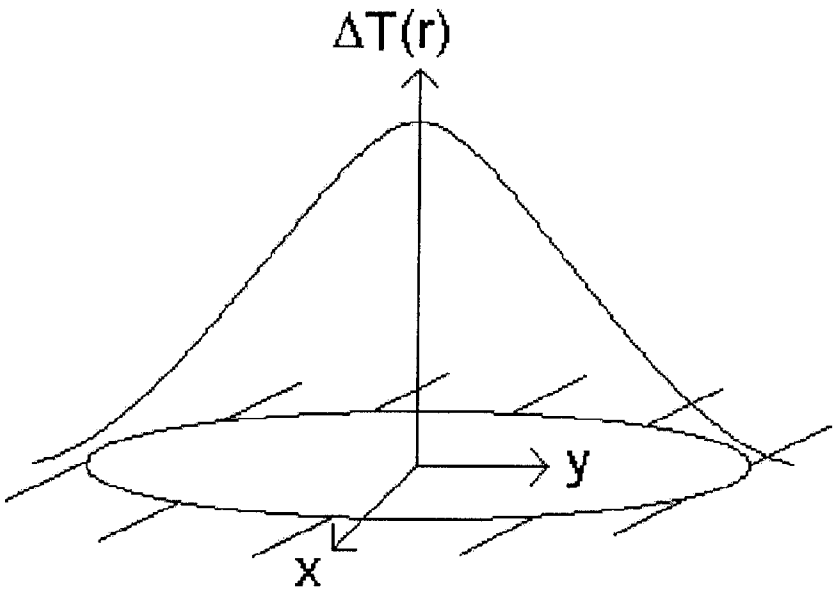

Figure 4-2: Normal Temperature Distribution over a Circular Plate

Safe Operating Criterion: Buckling of Circular Plates

The deformation δ from $\Delta T(r)$ is [19, 26, 27]

$$\begin{aligned}
\delta &= \int_0^R \alpha \Delta T(r) dr \\
&= \alpha \Delta T_m \int_0^R e^{-r^2/s^2} dr \\
&= \frac{\alpha \Delta T_m s \sqrt{\pi}}{2} erf(R/s)
\end{aligned}$$

Denoting $\Lambda = R/s$, the stress arising from $\Delta T(r)$ is therefore [19, 26, 27]

$$\begin{aligned}
\sigma_{th} &= -\sigma_{rr} \\
&= -\frac{E}{1-\nu}\frac{\delta}{R} \\
\Rightarrow \sigma_{th} &= -\frac{E}{1-\nu}\frac{\alpha \Delta T_m \sqrt{\pi} erf(\Lambda)}{2\Lambda}
\end{aligned}$$

Through eqn 3.25, eqn 3.6 and eqn 3.7, the maximum R before buckling failure is

$$R = \left\{ \frac{2.44Et^2\Lambda}{S(1+\nu)[E\alpha\Delta T_m\sqrt{\pi}erf(\Lambda) - 2\Lambda\sigma_{res}(1-\nu)]} \right\}^{1/2} \tag{4.8}$$

Heat Loss of Circular Plates

Eqn 3.35 provides the heat loss per unit area for a circular plate. For the normal temperature distribution, the boundary temperature ΔT_B at $r = R$ is

$$\Delta T_B = \Delta T_m e^{-\Lambda^2} \tag{4.9}$$

Power Generation of Circular Plates

Again, the normal temperature distribution will give a non-uniform power per unit area across the circular plate. To find the average power per unit area of the circular plate, first find the total power of a circular plate with radius R, then divide the total power by the area πR^2:

$$\begin{aligned} P &= \int_0^{2\pi}\int_0^R p(\Delta T(r))rdrd\theta \\ p_{ave} &= \frac{2\pi}{\pi R^2}\int_0^R prdr \\ \Rightarrow p_{ave} &= \frac{2}{R^2}\int_0^R prdr \end{aligned}$$

Substituting eqn 3.22 into the above equation,

$$p_{ave} = 2\left\{\frac{129025iR_g}{2F}\frac{1}{R^2}\int_0^R(\Delta T_m e^{-r^2/s^2}+T_{room})^{-0.2596}rdr \right.$$
$$-\frac{iR_g log2}{4F}\frac{1}{R^2}\int_0^R(\Delta T_m e^{-r^2/s^2}+T_{room})rdr$$
$$-i^2t\frac{1}{R^2}\int_0^R 10^{4.27\left(\frac{1000}{\Delta T_m e^{-r^2/s^2}+T_{room}}\right)-4.41}rdr$$
$$\left.-\frac{2iR_g\psi(i)}{F}\frac{1}{R^2}\int_0^R(\Delta T_m e^{-r^2/s^2}+T_{room})rdr\right\} \quad (4.10)$$

$$\Rightarrow p_{ave} = 2\left\{\frac{129025iR_g}{2F}\frac{1}{\Lambda^2}\int_0^\Lambda(\Delta T_m e^{-\zeta^2}+T_{room})^{-0.2596}\zeta d\zeta\right.$$
$$-\frac{iR_g log2}{8F\Lambda^2}[\Delta T_m(1-e^{-\Lambda^2})+T_{room}\Lambda^2]$$
$$-i^2t\frac{1}{\Lambda^2}\int_0^\Lambda 10^{4.27\left(\frac{1000}{\Delta T_m e^{-\zeta^2}+T_{room}}\right)-4.41}\zeta d\zeta$$
$$\left.-\frac{iR_g\psi(i)}{F\Lambda^2}[\Delta T_m(1-e^{-\Lambda^2})+T_{room}]\right\} \quad (4.11)$$

Net Power Generation of Structurally Stable Circular Plate

The net power generation is given by eqn 3.24, with average power generation given by eqn 4.11.

4.2 Comparison between Rectangular and Circular Plates

Two design spreadsheets are again constructed for normal temperature distribution across circular and rectangular plates. They are presented in Table 4.1 and Table 4.2.

Power generation between uniform and normal temperature distributions are compared by both temperature distributions having the same maximum temperature. For the choice of $\Lambda = 1.2$, the change in power generation and heat loss due to a change

Maximum Temperature of Temperature Profile (K)	Maximum Temperature Difference from Room Temperature of Temperature Profile (K)	Average Temperature Difference from Room Temperature Across Plate (K)	Temperature Difference from Room Temperature at Boundary (K)	Tensile=0, Compressive=1 at Operation	Does Maximum Radius Exist, If yes, Radius of Plate with Safety Factor (m)	q (W/m^2)	Ideal Current (A/m^2)	p (W/m^2)	p_{net}(W/m^2)
293	0	0	0	1	1.88E-06	0.0000E+00	0.000435114	2.7564E-04	2.7564E-04
373	80	53.78298615	18.95422069	1	1.67E-06	2.3958E+07	0.011966613	7.3268E-03	-2.3958E+07
423	130	87.39735249	30.80060863	1	1.57E-06	4.3764E+07	0.051021576	3.0585E-02	-4.3764E+07
473	180	121.0117188	42.64699658	1	1.48E-06	6.7242E+07	0.179290771	1.0566E-01	-6.7242E+07
523	230	154.6260852	54.4933845	1	1.41E-06	9.4361E+07	0.553894043	3.2058E-01	-9.4361E+07
573	280	188.2404515	66.33977243	1	1.35E-06	1.2509E+08	1.544189453	8.7963E-01	-1.2509E+08
593	300	201.686198	71.0783276	1	1.33E-06	1.3839E+08	2.270507813	1.2860E+00	-1.3839E+08
613	320	215.1319446	75.81688278	1	1.30E-06	1.5227E+08	3.295898438	1.8569E+00	-1.5227E+08
633	340	228.5776911	80.55543795	1	1.28E-06	1.6671E+08	4.730224609	2.6502E+00	-1.6671E+08
653	360	242.0234377	85.29399313	1	1.26E-06	1.8173E+08	6.713867188	3.7409E+00	-1.8173E+08
673	380	255.4691842	90.0325483	1	1.25E-06	1.9731E+08	9.436035156	5.2250E+00	-1.9731E+08
693	400	268.9148307	94.77110347	1	1.23E-06	2.1346E+08	13.11035156	7.2245E+00	-2.1346E+08
713	420	282.3606773	99.50965865	1	1.21E-06	2.3018E+08	18.06640625	9.8924E+00	-2.3018E+08
733	440	295.8064238	104.2482138	1	1.19E-06	2.4747E+08	24.609375	1.3418E+01	-2.4747E+08
753	460	309.2521703	108.986769	1	1.18E-06	2.6532E+08	33.25195313	1.8032E+01	-2.6532E+08
773	480	322.6979169	113.7253242	1	1.16E-06	2.8373E+08	44.53125	2.4011E+01	-2.8373E+08
788	495	332.7822268	117.2792405	1	1.15E-06	2.9791E+08	55.078125	2.9586E+01	-2.9791E+08
803	510	342.8665367	120.8331569	1	1.14E-06	3.1241E+08	67.67578125	3.6266E+01	-3.1241E+08
818	525	352.9508466	124.3870733	1	1.13E-06	3.2722E+08	82.8125	4.4223E+01	-3.2722E+08
833	540	363.0351565	127.9409897	1	1.12E-06	3.4235E+08	100.78125	5.3638E+01	-3.4235E+08
848	555	373.1194664	131.4949061	1	1.11E-06	3.5779E+08	122.0703125	6.4703E+01	-3.5779E+08
863	570	383.2037763	135.0488224	1	1.10E-06	3.7355E+08	146.875	7.7611E+01	-3.7355E+08
878	585	393.2880862	138.6027388	1	1.09E-06	3.8962E+08	175.78125	9.2555E+01	-3.8962E+08
893	600	403.3723961	142.1566552	1	1.08E-06	4.0600E+08	209.1796875	1.0971E+02	-4.0600E+08
908	615	413.456706	145.7105716	1	1.07E-06	4.2270E+08	247.5585938	1.2925E+02	-4.2270E+08
923	630	423.5410159	149.264488	1	1.06E-06	4.3972E+08	291.2109375	1.5128E+02	-4.3972E+08
938	645	433.8253258	152.8184043	1	1.06E-06	4.5704E+08	339.84375	1.7591E+02	-4.5704E+08

Table 4.1: Design Spreadsheet for Normal Temperature Distributions over a Circular Plate

Maximum Temperature of Temperature Profile (K)	Maximum Temperature Difference from Room Temperature of Temperature Profile (K)	Average Temperature Difference from Room Temperature Across Plate (K)	Temperature Difference from Room Temperature at Boundary (K)	Tensile=0, Compressive=1 at Operation	Does Maximum Side Length Exist, if yes, 0.5*Side Length of Plate with Safety Factor, or "I"(m)	q (W/m^2)	Ideal Current (A/m^2)	p (W/m^2)	p_{net}(W/m^2)
293	0	0	0	1	1.54E-06	0.0000E+00	0.000435114	2.7564E-04	2.7564E-04
373	80	53.78298389	18.95422069	1	1.38E-06	1.6915E+08	0.020098686	1.2188E-02	-1.6915E+08
423	130	87.39734883	30.80060863	1	1.31E-06	2.9132E+08	0.089836121	5.3221E-02	-2.9132E+08
473	180	121.0117136	42.64699656	1	1.24E-06	4.2493E+08	0.322723389	1.8685E-01	-4.2493E+08
523	230	154.6260787	54.4933845	1	1.18E-06	5.6916E+08	1.005554199	5.7064E-01	-5.6916E+08
573	280	188.2404436	66.33977243	1	1.13E-06	7.2342E+08	2.813720703	1.5694E+00	-7.2342E+08
593	300	201.6861896	71.0783276	1	1.11E-06	7.8779E+08	4.144287109	2.2949E+00	-7.8779E+08
613	320	215.1319356	75.81688278	1	1.10E-06	8.5364E+08	6.030273438	3.3133E+00	-8.5364E+08
633	340	228.5776815	80.55543795	1	1.08E-06	9.2093E+08	8.654785156	4.7265E+00	-9.2093E+08
653	360	242.0234275	85.29399313	1	1.06E-06	9.8964E+08	12.28027344	6.6658E+00	-9.8964E+08
673	380	255.4691735	90.0325483	1	1.05E-06	1.0598E+09	17.23632813	9.2982E+00	-1.0598E+09
693	400	268.9149195	94.77110347	1	1.03E-06	1.1312E+09	23.97460938	1.2833E+01	-1.1312E+09
713	420	282.3606654	99.50965865	1	1.02E-06	1.2040E+09	32.91015625	1.7529E+01	-1.2040E+09
733	440	295.8064114	104.2482138	1	1.01E-06	1.2782E+09	44.77539063	2.3898E+01	-1.2782E+09
753	460	309.2521574	108.986769	1	9.94E-07	1.3536E+09	60.25390625	3.1709E+01	-1.3536E+09
773	480	322.6979034	113.7253242	1	9.82E-07	1.4304E+09	80.2734375	4.1985E+01	-1.4304E+09
788	495	332.7822126	117.2792405	1	9.73E-07	1.4887E+09	98.828125	5.1480E+01	-1.4887E+09
803	510	342.8665223	120.8331569	1	9.64E-07	1.5478E+09	120.703125	6.2679E+01	-1.5478E+09
818	525	352.9508318	124.3870733	1	9.56E-07	1.6076E+09	146.875	7.5851E+01	-1.6076E+09
833	540	363.0351413	127.9409897	1	9.47E-07	1.6680E+09	177.34375	9.1174E+01	-1.6680E+09
848	555	373.1194508	131.4949061	1	9.39E-07	1.7291E+09	212.6953125	1.0883E+02	-1.7291E+09
863	570	383.2037602	135.0488224	1	9.31E-07	1.7909E+09	253.125	1.2895E+02	-1.7909E+09
878	585	393.2880697	138.6027388	1	9.23E-07	1.8534E+09	298.828125	1.5164E+02	-1.8534E+09
893	600	403.3723792	142.1566552	1	9.16E-07	1.9165E+09	350.78125	1.7693E+02	-1.9165E+09
908	615	413.4566887	145.7105716	1	9.09E-07	1.9803E+09	408.203125	2.0479E+02	-1.9803E+09
923	630	423.5409982	149.264488	1	9.01E-07	2.0447E+09	472.65625	2.3511E+02	-2.0447E+09
938	645	433.6253076	152.8184043	1	8.94E-07	2.1097E+09	542.578125	2.6773E+02	-2.1097E+09

Table 4.2: Design Spreadsheet for Normal Temperature Distributions over a Rectangular Plate

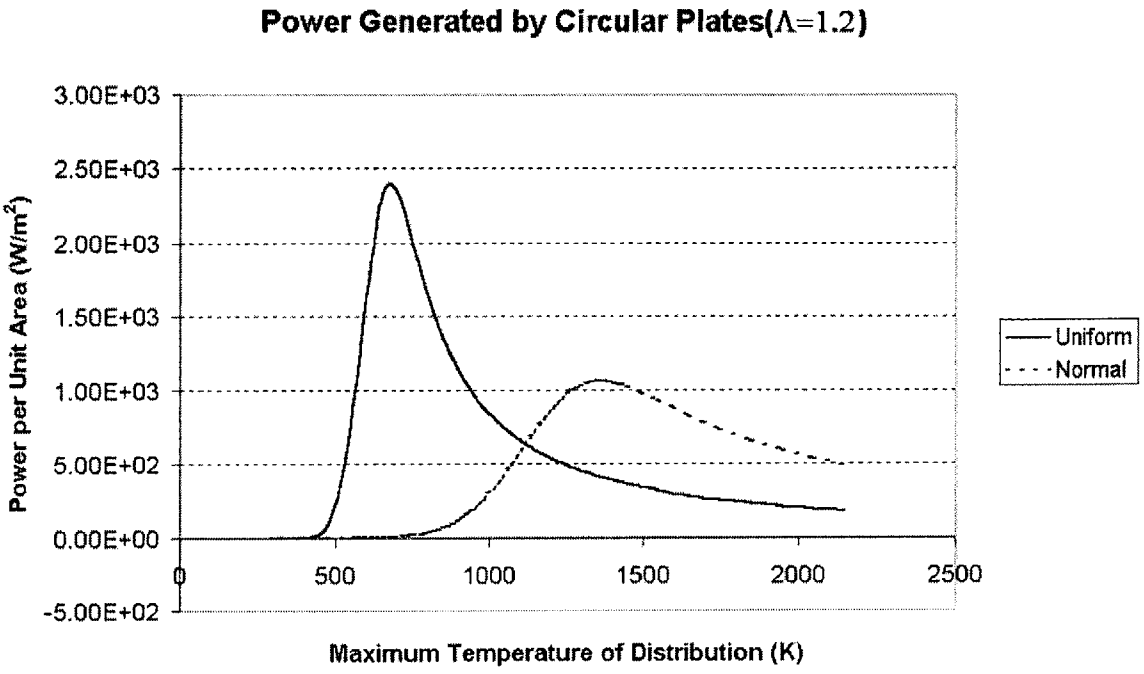

Figure 4-3: Power Generation of Stable Circular Plates under Uniform and Normal Temperature Distributions

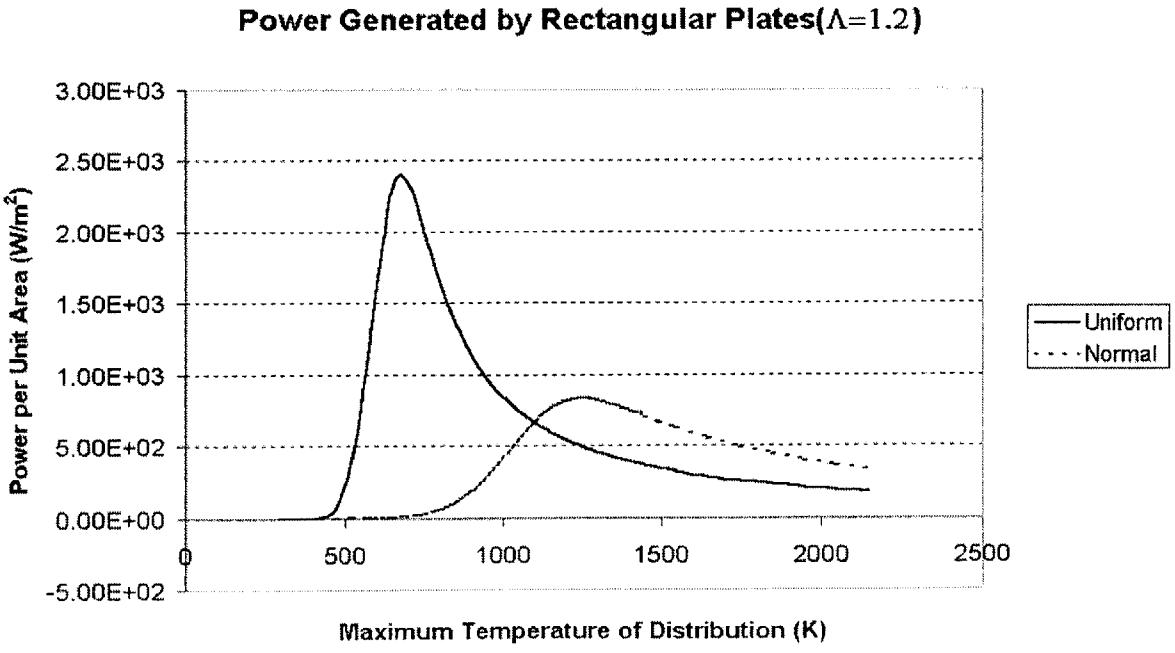

Figure 4-4: Power Generation of Stable Rectangular Plates under Uniform and Normal Temperature Distributions

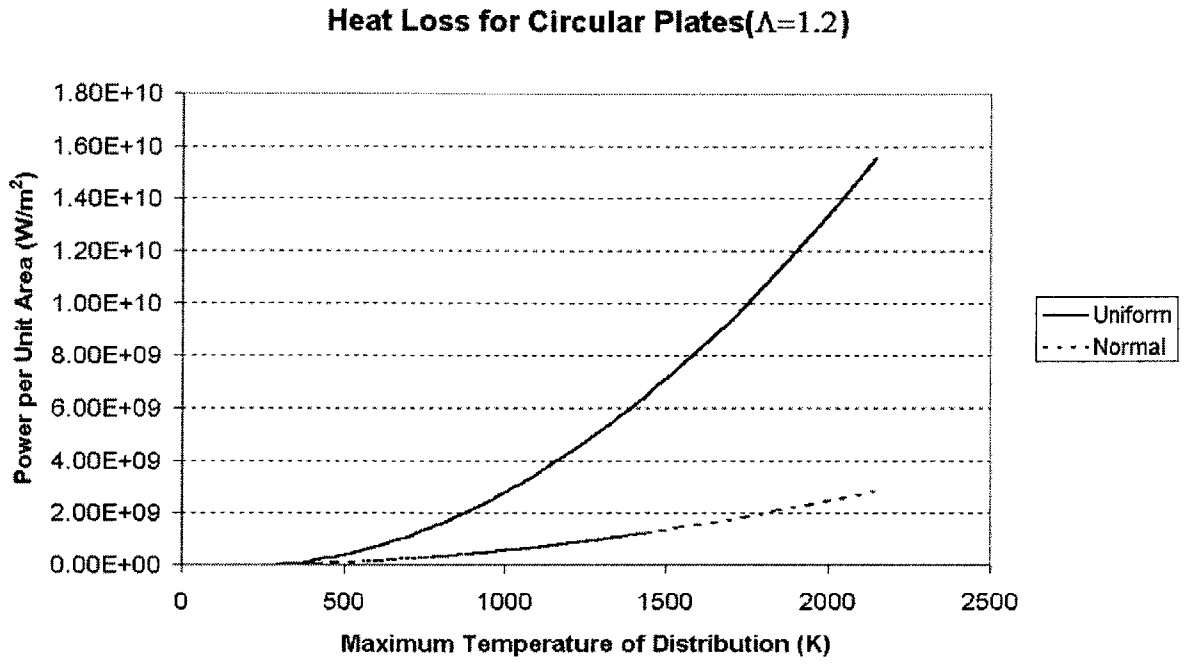

Figure 4-5: Heat Loss of Stable Circular Plates under Uniform and Normal Temperature Distributions

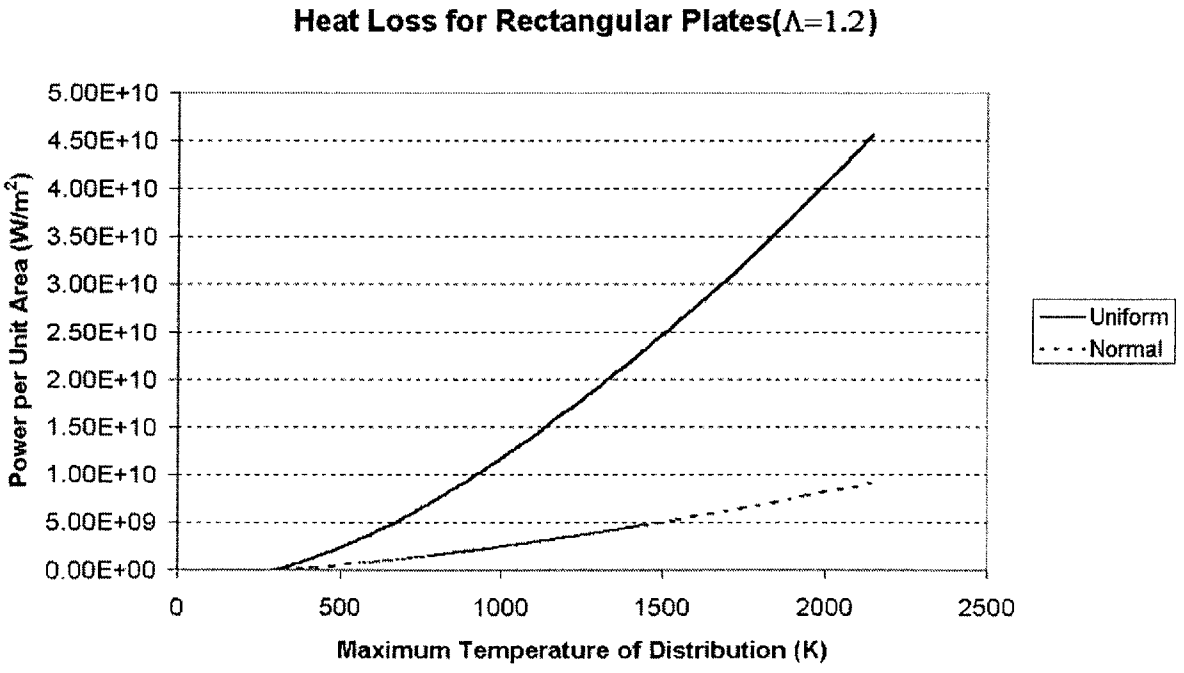

Figure 4-6: Heat Loss of Stable Rectangular Plates under Uniform and Normal Temperature Distributions

from uniform to normal temperature distribution is similar for both plate geometries. Observing Figure 4-3 to Figure 4-6, although the change in temperature distribution decreases heat loss from the plates, it also causes a decrease in maximum power generated. This is accounted for by portions of the plate having lower temperatures in a normal temperature distribution, thus decreasing the power generated in those portions. An ideal temperature distribution would therefore consist of a portion where the temperature is constant over the plate center to maximize power generation, and at the boundary the temperature would taper off to close to room temperature to minimize heat loss. This temperature distribution can be considered to be a hybrid between the uniform temperature distribution and the normal temperature distribution, and such a hybrid temperature distribution is considered in the next section.

4.3 Modeling of Micro-fabricated SOFC: Hybrid Temperature Distribution

The analysis for the hybrid temperature distribution will again be performed for a rectangular and a circular plate.

4.3.1 Rectangular Plates

The hybrid temperature distribution over a rectangular plate is shown in the following equation and Figure 4-7:

$$\Delta T(y) = \begin{cases} \Delta T_m, \text{ if } 0 < |y| < y' \\ \Delta T_m e^{-\frac{(y-y')^2}{s^2}}, \text{ if } |y| > y' \end{cases}$$

The four-step analysis process is now carried out for this temperature distribution.

Safe Operating Criterion: Buckling of Rectangular Plates

The deformation δ resulting from this temperature distribution is

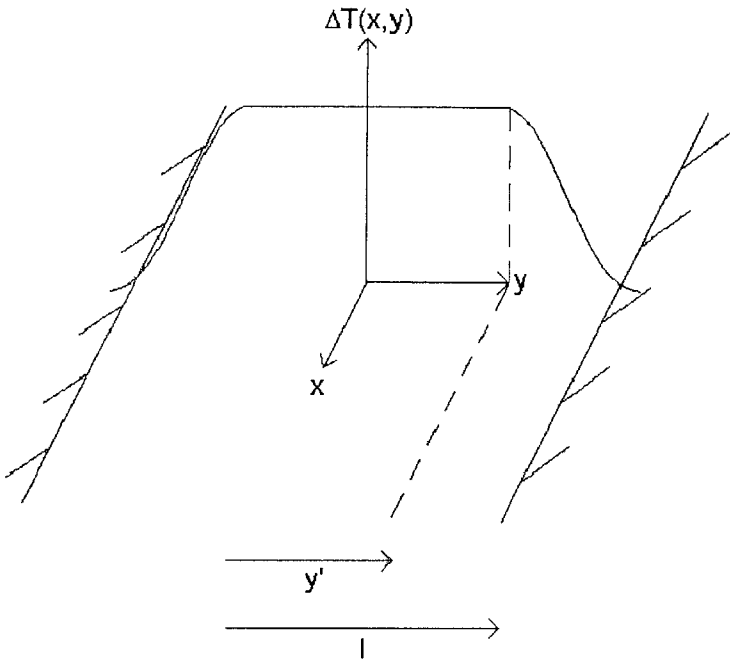

Figure 4-7: Hybrid Temperature Distribution over a Rectangular Plate

$$\begin{aligned}
\delta &= \int_0^l \alpha \Delta T(y) dy \\
&= \alpha \left[\int_0^{y'} \Delta T_m dy + \int_{y'}^{l} \Delta T_m e^{-\frac{(y-y')^2}{s^2}} dy \right] \\
&= \alpha \left[\Delta T_m y' + s \Delta T_m \int_0^{l/s - y'/s} e^{-\zeta^2} d\zeta \right]
\end{aligned}$$

Denoting $\Lambda = l/s$ and $\lambda = y'/s$,

$$\Rightarrow \delta = \alpha \Delta T_m y' + \frac{\Delta T_m \alpha \sqrt{\pi}}{2} serf(\Lambda - \lambda) \tag{4.12}$$

σ_{th} is then

$$\begin{aligned}\sigma_{th} &= -\frac{E}{1-\nu}\frac{\delta}{l} \\ &= -\frac{E}{1-\nu}\left[\alpha\Delta T_m\frac{y'}{l}+\frac{\Delta T_m\alpha\sqrt{\pi}}{2}\frac{s}{l}erf(\Lambda-\lambda)\right] \\ &= -\frac{E\alpha}{1-\nu}\left[\Delta T_m\left(\frac{\lambda}{\Lambda}\right)+\frac{\Delta T_m\sqrt{\pi}}{2\Lambda}erf(\Lambda-\lambda)\right]\end{aligned}$$

Using eqn 3.6, eqn 3.7 and eqn 3.3, the maximum rectangular plate side length that avoids buckling is

$$l=\left\{\frac{2\Lambda E\pi^2t^2}{12S(1+\nu)\{E\alpha\Delta T_m[2\lambda+\sqrt{\pi}erf(\Lambda-\lambda)]-2\Lambda\sigma_{res}(1-\nu)\}}\right\}^{1/2} \tag{4.13}$$

Similar to the case for a normal temperature distribution, Λ and λ are non-dimensional variables that define the hybrid temperature distribution. They are used in place of y' and s to simplify calculation.

Heat Loss of Rectangular Plates

Heat loss of this rectangular plate is again given by eqn 3.19. The boundary temperature of the rectangular plate for this temperature distribution is

$$\begin{aligned}\Delta T_B &= \Delta T_m e^{-\frac{(l-y')^2}{s^2}} \\ &= \Delta T_m e^{-\frac{l^2}{s^2}\left(1-\frac{y'}{l}\right)^2} \\ \Rightarrow \Delta T_B &= \Delta T_m e^{-\Lambda^2\left(1-\frac{\lambda}{\Lambda}\right)^2}\end{aligned}$$

Power Generation of Rectangular Plates

The average power per unit area is found through the following expression:

$$p_{ave}=\frac{1}{l}\left(\int_0^{y'}pdy+\int_{y'}^{l}pdy\right) \tag{4.14}$$

Using eqn 3.22, the above integration results in

$$p_{ave} = \frac{\lambda}{\Lambda}\left[\frac{129025iR_g}{2F}(\Delta T_m + T_{room})^{-0.2596} - \frac{iR_g log2}{4F}(\Delta T_m + T_{room}) - i^2 t 10^{4.27\left(\frac{1000}{\Delta T_m + T_{room}}\right)-4.41} - \frac{2iR_g}{F}(\Delta T_m + T_{room})\psi(i)\right] + \frac{129025iR_g}{2F}\frac{1}{\Lambda}\int_0^{\Lambda-\lambda}(\Delta T_m e^{-\zeta^2} + T_{room})^{-0.2596}d\zeta - \frac{iR_g log2}{8F\Lambda}\left[\Delta T_m\sqrt{\pi}erf(\Lambda-\lambda) + 2\Lambda T_{room}\left(1-\frac{\lambda}{\Lambda}\right)\right] - i^2 t\frac{1}{\Lambda}\int_0^{\Lambda-\lambda} 10^{4.27\left(\frac{1000}{\Delta T_m e^{-\zeta^2} + T_{room}}\right)-4.41}d\zeta - \frac{iR_g\psi(i)}{F\Lambda}\left[\Delta T_m\sqrt{\pi}erf(\Lambda-\lambda) + 2\Lambda T_{room}\left(1-\frac{\lambda}{\Lambda}\right)\right] \quad (4.15)$$

Net Power Generation of Rectangular Plates

The net power per unit area is given by eqn 3.24, using the average power calculated from eqn 4.15.

4.3.2 Circular Plates

The hybrid temperature distribution over a circular plate is given by

$$\Delta T_r = \begin{cases} \Delta T_m, \text{ if } 0 < r < r' \\ \Delta T_m e^{-\frac{(r-r')^2}{s^2}}, \text{ if } r > r' \end{cases}$$

The temperature distribution is also shown in Figure 4-8.

Safe Operating Criterion: Buckling of Circular Plates

The deformation δ of the circular plate associated with the hybrid temperature distribution is

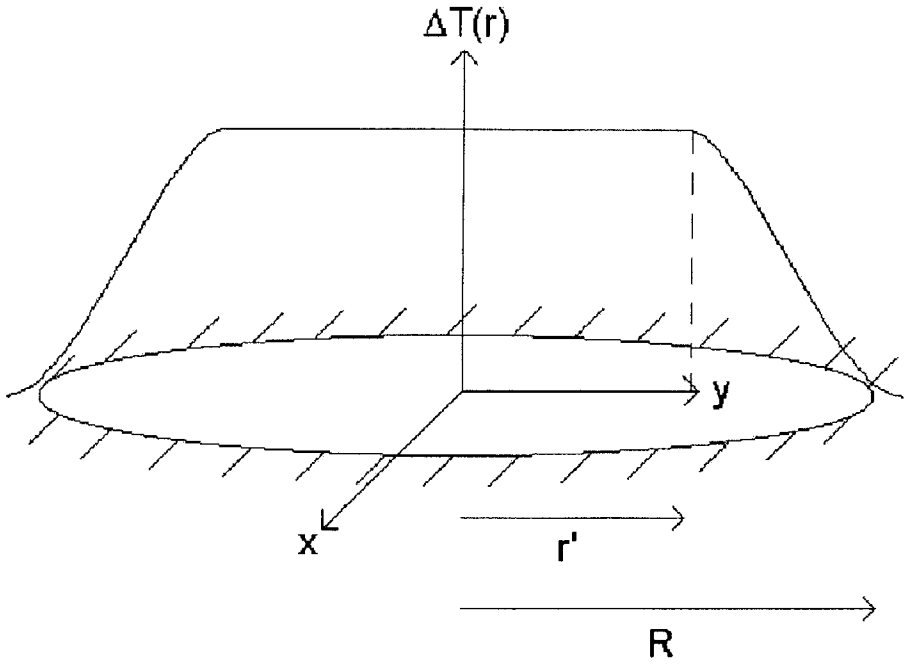

Figure 4-8: Hybrid Temperature Distribution over a Circular Plate

$$\begin{aligned}
\delta &= \int_0^R \alpha \Delta T(r) dr \\
&= \alpha \left[\Delta T_m r' + \int_{r'}^R \Delta T_m e^{-\frac{(r-r')^2}{s^2}} dr \right] \\
&= \alpha \Delta T_m \left[r' + \frac{s\sqrt{\pi}}{2} erf(\Lambda - \lambda) \right]
\end{aligned}$$

The stress from this deformation is then

$$\begin{aligned}
\sigma_{th} &= -\sigma_{rr} \\
&= -\frac{E}{1-\nu}\frac{\delta}{R} \\
&= -\frac{E\alpha\Delta T_m}{2\Lambda(1-\nu)}[2\lambda + \sqrt{\pi} erf(\Lambda - \lambda)]
\end{aligned}$$

Therefore the maximum R that just avoids buckling failure is

$$R = \left\{ \frac{2.44\Lambda E t^2}{S(1+\nu)\{E\alpha\Delta T_m[2\lambda + \sqrt{\pi} erf(\Lambda - \lambda)] - 2\sigma_{res}\Lambda(1-\nu)\}} \right\}^{1/2} \tag{4.16}$$

Heat Loss of Circular Plates

The heat loss of this circular plate is given by eqn 3.35. The boundary temperature in this equation is in turn given by

$$\Delta T_B = \Delta T_m e^{-\Lambda^2\left(1-\frac{\lambda}{\Lambda}\right)^2} \tag{4.17}$$

Power Generation of Circular Plates

Similar to the previous chapter on the average power generation of circular plates, the average power generated for a circular plate under such a temperature distribution is given by the following expression:

$$p_{ave} = \frac{2}{R^2}\left(\int_0^{r'} prdr + \int_{r'}^{R} prdr\right) \tag{4.18}$$

The above equation results in

$$p_{ave} = \left(\frac{\lambda}{\Lambda}\right)^2 \left[\frac{129025iR_g}{2F}(\Delta T_m + T_{room})^{-0.2596} - \frac{iR_g log2}{4F}(\Delta T_m + T_{room}) - i^2 t 10^{4.27\left(\frac{1000}{\Delta T_m + T_{room}}\right)-4.41} - \frac{2iR_g\psi(i)}{F}(\Delta T_m + T_{room})\right] + \frac{129025iR_g}{F}\frac{1}{\Lambda^2}\int_0^{\Lambda-\lambda}(\Delta T_m e^{-\zeta^2} + T_{room})^{-0.2596}(\zeta+\lambda)d\zeta - \frac{iR_g log2}{4F\Lambda^2}\{\Delta T_m[1-e^{-(\Lambda-\lambda)^2}] + T_{room}(\Lambda-\lambda)^2 + \Delta T_m\lambda\sqrt{\pi}erf(\Lambda-\lambda) + 2\lambda T_{room}(\Lambda-\lambda)\} - 2i^2 t\frac{1}{\Lambda^2}\int_0^{\Lambda-\lambda} 10^{4.27\left(\frac{1000}{\Delta T_m e^{-\zeta^2} + T_{room}}\right)-4.41}(\zeta+\lambda)d\zeta - \frac{2iR_g\psi(i)}{F\Lambda^2}\{\Delta T_m[1-e^{-(\Lambda-\lambda)^2}] + T_{room}(\Lambda-\lambda)^2 + \Delta T_m\lambda\sqrt{\pi}erf(\Lambda-\lambda) + 2\lambda T_{room}(\Lambda-\lambda)\} \tag{4.19}$$

Net Power Generation of Circular Plates

The net power generation is given by eqn 3.24 and average power by eqn 4.19.

4.3.3 Comparison between Rectangular and Circular Plates

Two design spreadsheets are presented in Table 4.3 and Table 4.4.

Again, the behavior of the power generated and the heat loss under the hybrid temperature distribution is similar for both plate geometries: The change from a normal temperature distribution to a hybrid temperature distribution causes an increase in the maximum power generated. However, the heat loss is higher than that of normal temperature distribution. This can be explained by understanding that under a hybrid temperature distribution, more of the plate is at a high temperature than under a normal temperature distribution. Therefore the size of a plate under a hybrid temperature distribution must be smaller than one under a normal temperature distribution for the plate to be stable, increasing the heat loss per unit area of the plate [35].

Although the analyses performed on two plate geometries under three diffferent tem-

Maximum Temperature of Temperature Profile (K)	Maximum Temperature Difference from Room Temperature of Temperature Profile (K)	Average Temperature Difference from Room Temperature Across Plate (K)	Temperature Difference from Room Temperature at Boundary (K)	Tensile=0, Compressive=1 at Operation	Does Maximum Radius Exist, if yes, Radius of Plate with Safety Factor (m)	q (W/m^2)	Ideal Current (A/m^2)	p (W/m^2)	p_{net}(W/m^2)
293	0	0	0	1	1.68124E-06	0.0000E+00	0.000435114	0.00027564	2.7564E-04
373	80	65.16637101	32.44436041	1	1.65132E-06	4.1851E+07	0.047016144	0.02846188	-4.1851E+07
423	130	105.8953529	52.72208586	1	1.54428E-06	7.7117E+07	0.366973877	0.216334408	-7.7117E+07
473	180	146.6243348	72.99981091	1	1.45567E-06	1.1930E+08	2.07824707	1.198018214	-1.1930E+08
523	230	187.3533167	93.27753616	1	1.38076E-06	1.6834E+08	9.375	5.286205282	-1.6834E+08
573	280	228.0822985	113.5552614	1	1.31633E-06	2.2418E+08	35.15625	19.44695348	-2.2418E+08
593	300	244.3738913	121.6663515	1	1.29297E-06	2.4840E+08	56.93359375	31.27659363	-2.4840E+08
613	320	260.6654841	129.7774416	1	1.27082E-06	2.7371E+08	89.94140625	49.03309312	-2.7371E+08
633	340	276.9570768	137.8885317	1	1.24976E-06	3.0010E+08	138.28125	74.86614343	-3.0010E+08
653	360	293.2486696	145.9996218	1	1.22972E-06	3.2755E+08	206.8359375	111.1841194	-3.2755E+08
673	380	309.5402623	154.1107119	1	1.21061E-06	3.5606E+08	300.78125	160.3176967	-3.5606E+08
693	400	325.8318551	162.221802	1	1.19237E-06	3.8567E+08	424.8046875	224.063039	-3.8567E+08
713	420	342.1234478	170.3328921	1	1.17492E-06	4.1634E+08	583.0078125	303.2570704	-4.1634E+08
733	440	358.4150406	178.4439822	1	1.15822E-06	4.4806E+08	778.125	397.5545671	-4.4806E+08
753	460	374.7066333	186.5550723	1	1.14222E-06	4.8085E+08	1016.210938	505.4179075	-4.8085E+08
773	480	390.9982261	194.6661624	1	1.12685E-06	5.1470E+08	1292.382813	624.2100346	-5.1470E+08
788	495	403.2169206	200.74948	1	1.11573E-06	5.4078E+08	1528.125	718.3407147	-5.4078E+08
803	510	415.4356152	206.8327976	1	1.10493E-06	5.6746E+08	1785.9375	814.7825766	-5.6746E+08
818	525	427.6543098	212.9161152	1	1.09444E-06	5.9473E+08	2063.085938	911.5014509	-5.9473E+08
833	540	439.8730043	218.9994327	1	1.08424E-06	6.2259E+08	2353.125	1006.318741	-6.2259E+08
848	555	452.0916989	225.0827503	1	1.07432E-06	6.5104E+08	2657.8125	1097.001474	-6.5104E+08
863	570	464.3103935	231.1660679	1	1.06467E-06	6.8009E+08	2964.84375	1181.359521	-6.8009E+08
878	585	476.529088	237.2493855	1	1.05527E-06	7.0973E+08	3267.773438	1257.377041	-7.0973E+08
893	600	488.7477826	243.332703	1	1.04612E-06	7.3996E+08	3557.8125	1323.333904	-7.3996E+08
908	615	500.9664772	249.4160206	1	1.0372E-06	7.7078E+08	3823.828125	1377.919642	-7.7077E+08
923	630	513.1851717	255.4993382	1	1.02851E-06	8.0218E+08	4067.96875	1420.326163	-8.0218E+08
938	645	525.4038663	261.5826558	1	1.02003E-06	8.3418E+08	4266.40625	1450.277517	-8.3418E+08

Table 4.3: Design Spreadsheet for Hybrid Temperature Distributions over a Circular Plate

Maximum Temperature of Temperature Profile (K)	Maximum Temperature Difference from Room Temperature of Temperature Profile (K)	Average Temperature Difference from Room Temperature Across Plate (K)	Temperature Difference from Room Temperature at Boundary (K)	Tensile=0, Compressive=1 at Operation	Does Maximum Side Length Exist, if yes, 0.5*Side Length of Plate with Safety Factor, or 'T'(m)	q (W/m^2)	Ideal Current (A/m^2)	p (W/m^2)	p_{net}(W/m^2)
293	0	0	0	1	1.54462E-06	0.0000E+00	0.000435114	0.00027564	2.7564E-04
373	80	65.1663691	32.44436041	1	1.35585E-06	2.8552E+08	0.07666615	0.04617058	-2.9552E+08
423	130	105.8953498	52.72208586	1	1.26796E-06	5.1350E+08	0.638580322	0.37315028	-5.1350E+08
473	180	146.6243305	72.99981091	1	1.19521E-06	7.5426E+08	3.7109375	2.11306424	-7.5426E+08
523	230	187.3533112	93.27753616	1	1.1337E-06	1.0161E+09	16.89453125	9.39472282	-1.0161E+09
573	280	228.0822919	113.5552614	1	1.0808E-06	1.2975E+09	63.18359375	34.4181541	-1.2975E+09
593	300	244.3738841	121.6663515	1	1.06162E-06	1.4153E+09	101.7578125	54.9813011	-1.4153E+09
613	320	260.6654764	129.7774416	1	1.04343E-06	1.5359E+09	158.984375	85.2558268	-1.5359E+09
633	340	276.9570687	137.8885317	1	1.02614E-06	1.6594E+09	240.8203125	128.003783	-1.6594E+09
653	360	293.248661	145.9996218	1	1.00968E-06	1.7857E+09	353.125	185.683176	-1.7857E+09
673	380	309.5402532	154.1107119	1	9.93994E-07	1.9146E+09	500.390625	259.756769	-1.9146E+09
693	400	325.8318455	162.221802	1	9.79014E-07	2.0462E+09	686.328125	350.229428	-2.0462E+09
713	420	342.1234378	170.3328921	1	9.64691E-07	2.1804E+09	916.015625	455.512581	-2.1804E+09
733	440	358.4150301	178.4439822	1	9.5098E-07	2.3172E+09	1188.28125	572.528858	-2.3172E+09
753	460	374.7066223	188.5550723	1	9.37837E-07	2.4564E+09	1503.125	696.927128	-2.4564E+09
773	480	390.9982146	194.6661624	1	9.25224E-07	2.5982E+09	1851.757813	823.355755	-2.5982E+09
788	495	403.2169088	200.74948	1	9.16091E-07	2.7061E+09	2135.546875	915.915995	-2.7061E+09
803	510	415.435603	206.8327976	1	9.07224E-07	2.8153E+09	2421.875	1003.6401	-2.8153E+09
818	525	427.6542972	212.9161152	1	8.98609E-07	2.9259E+09	2717.96875	1084.02271	-2.9259E+09
833	540	439.8729914	218.9994327	1	8.90235E-07	3.0378E+09	3003.125	1154.81739	-3.0378E+09
848	555	452.0916856	225.0827503	1	8.82091E-07	3.1510E+09	3274.21875	1214.21781	-3.1510E+09
863	570	464.3103798	231.1660679	1	8.74166E-07	3.2655E+09	3515.625	1260.99606	-3.2655E+09
878	585	476.529074	237.2493855	1	8.66451E-07	3.3813E+09	3725.78125	1294.58629	-3.3813E+09
893	600	488.7477683	243.332703	1	8.58937E-07	3.4983E+09	3884.765625	1315.12017	-3.4983E+09
908	615	500.9664625	249.4160206	1	8.51615E-07	3.6166E+09	4003.90625	1323.34825	-3.6166E+09
923	630	513.1851567	255.4993382	1	8.44478E-07	3.7361E+09	4083.984375	1320.53804	-3.7361E+09
938	645	525.4038509	261.5826558	1	8.37516E-07	3.8569E+09	4101.5625	1308.29149	-3.8569E+09

Table 4.4: Design Spreadsheet for Hybrid Temperature Distributions over a Rectangular Plate

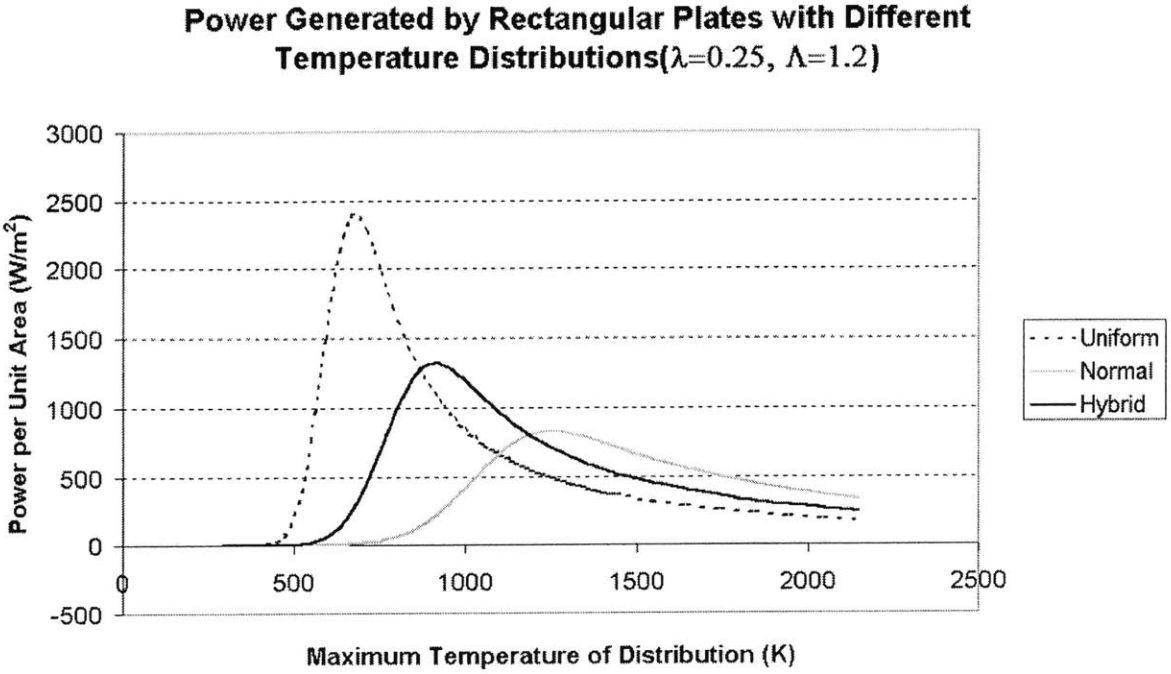

Figure 4-9: Power Generated for Stable Rectangular Plates under Uniform, Normal and Hybrid Temperature Distributions

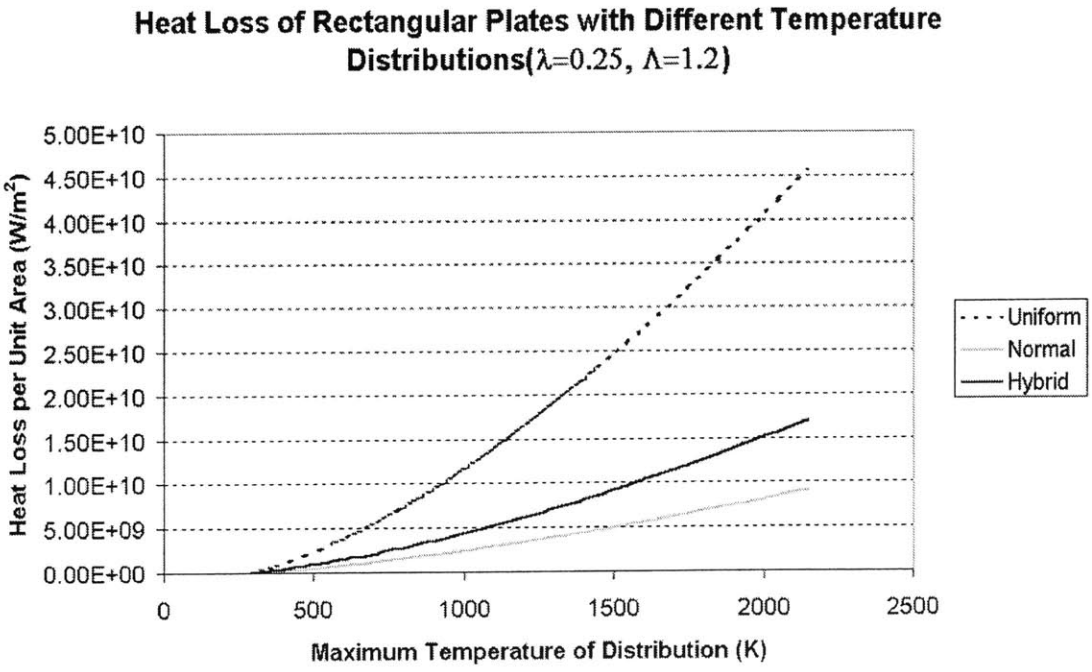

Figure 4-10: Heat Loss for Stable Rectangular Plates under Uniform, Normal and Hybrid Temperature Distributions

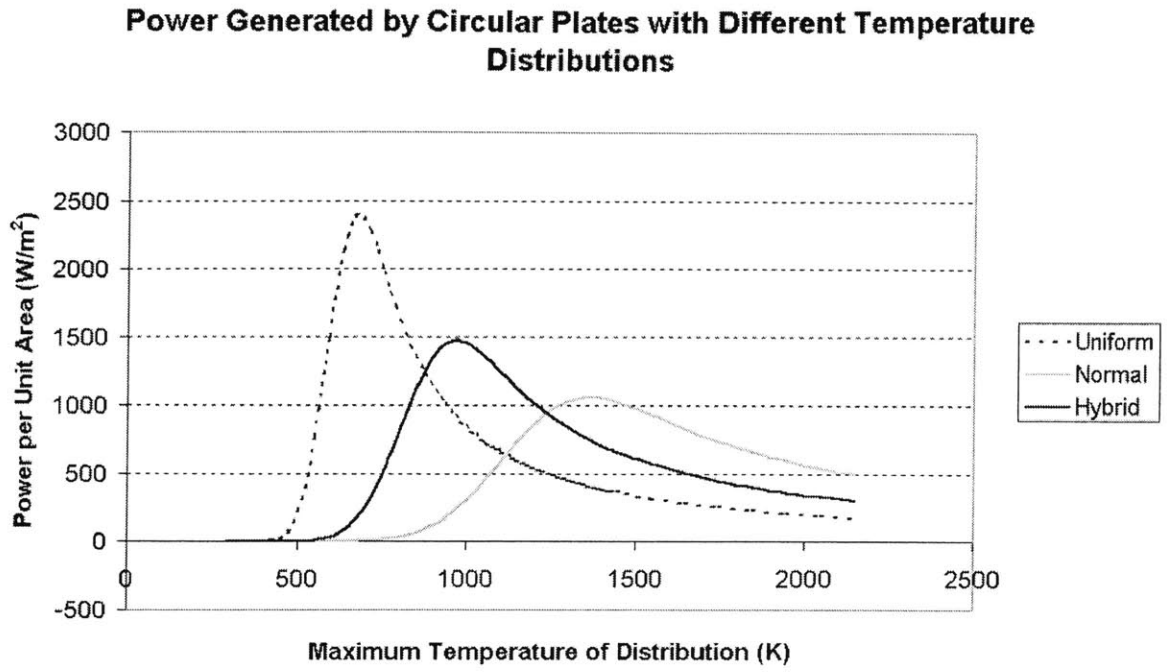

Figure 4-11: Power Generated for Stable Circular Plates under Uniform, Normal and Hybrid Temperature Distributions

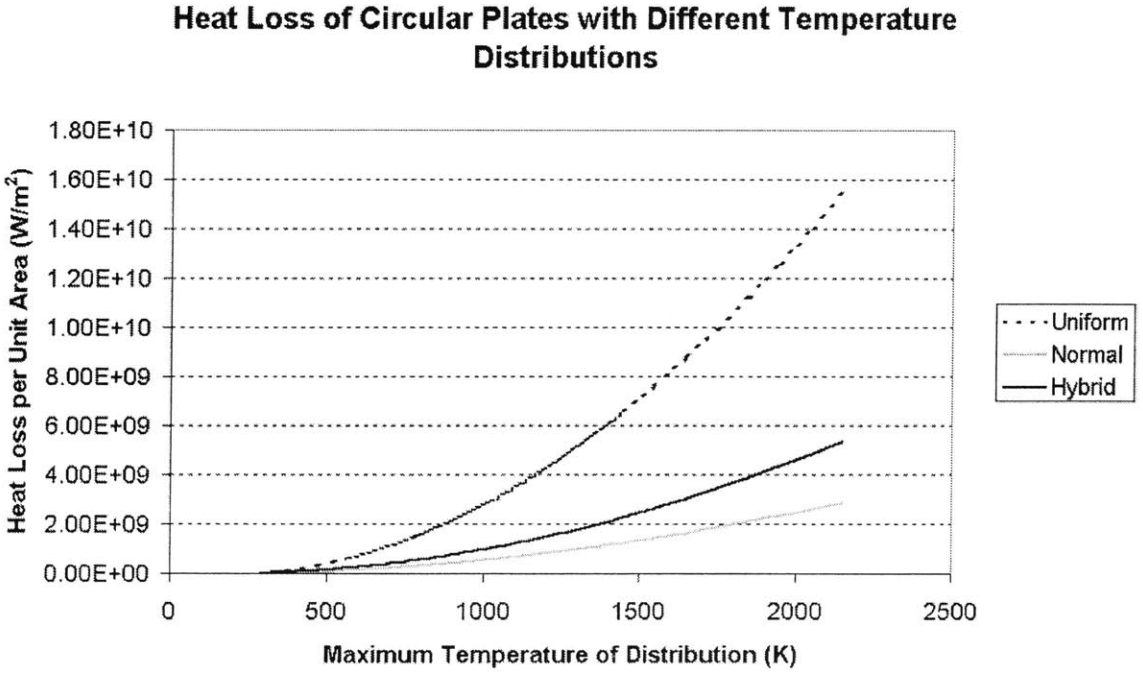

Figure 4-12: Heat Loss for Stable Circular Plates under Uniform, Normal and Hybrid Temperature Distributions

perature distributions have suggested pessimistic power generation capabilities for the current SOFC design(with the heat loss out of the plate larger than the power generated by approximately $10^6 W/m^2$), a functioning design can still be realized if a high degree of thermal isolation can be achieved.

Chapter 5

Conclusions, and Future Investigations for Micro-Chemical SOFC Modeling

From the preceding analyses, it was shown that power generated and heat loss differ by a factor of approximately 10^6, with power generated smaller than heat loss. It is therefore apparent that the current design will not be able to produce net power; either power generated must be increased or heat loss must be decreased.

As for the geometry of the plates, although circular plates proved to have a lower heat loss than that of rectangular plates, the heat losses for the two different geometries are nevertheless still comparable(Heat loss per unit area for rectangular plates is approximately four times that of circular plates, both under uniform temperature distribution at 800K). Furthermore, the buckling ΔT for rectangular and circular plates are also comparable(For plate thickness of 1 micron, buckling ΔT for rectangular plates with aspect ratio of a/b=2.5 differ from that for circular plates by approximately a factor of 2). Therefore at this stage the only criterion for selecting the plate geometry is through the ease of fabrication [21]. However, it seems to be the case that altering the plate geometry will not be sufficient to render p_{net} positive. Although the analyses reported a rather pessimistic picture for the current design, nevertheless a systematic technique is developed in this thesis to solve the coupled

problem: The initial problem is broken down into analyses of mechanical stability, heat loss, power generation, and finally the results are integrated together to provide an evaluation of power generation capabilities of stable designs. This systematic technique can be adapted to future design analyses and evaluations.

Several topics for future investigation follow from the conclusions drawn previously. To investigate the possibility of increasing power generation, it is important to note that the power generation of a YSZ plate is governed by eqn 3.20. It is possible that for other electrolyte candidates the components in eqn 3.20 are different, and these other candidates may prove to produce more power than YSZ. Alternatively, the prospect of heat loss minimization through better insulation or employing non-planar structures such as tubes should also be investigated for the purposes of increasing p_{net} [14, 9, 25, 12].

The next set of future topics attempts to improve the accuracy of the model. One topic that must be investigated is the heat generation from the water formation reaction, as this would make the model much more accurate [17, 6]. Next, confidence in the models developed can be increased by verifying the material properties used in the models through experiments. It is well known that the properties of materials such as YSZ are highly dependent upon processing conditions, therefore there is no guarantee that the material properties obtained from literature are the same as those in the model developed [9].

Finally the model itself can be made more useful by interfacing it with the system-level models. This is because although the fuel cell is the part of the device that generates power, other aspects of the device such as fuel/oxygen management is also important to the overall power generation. Therefore the interfacing between the fuel-cell-level and the system-level models will make the overall design process more convenient.

Appendix A

Nomenclature

Temperature	
ΔT	Temperature change from room temperature
ΔT_b	Temperature change for buckling
ΔT_f	Temperature change for fracture
ΔT_B	Temperature difference between the plate boundary and room temperature
ΔT_m	Difference between maximum temperature of the temperature distribution and room temperature
T_{op}	Operation temperature
T_B	Boundary Temperature
T_{room}	Room Temperature

Table A.1: Temperature-Related Symbols and Their Definitions

Dimensional/Non-Dimensional Lengths	
t	Thickness
a	Plate length
b	Plate width
γ	a/b
$w(x, y)$	Deflection in the z-direction (Out-of-plane deflection)
w_0	Arbitrary constant for deflection profile
l	Half of plate side length
L	Half of silicon die side length
ζ	t/l
β	Dummy length variable
r	Radial coordinate
R	Plate radius
s	Standard deviation
δ	Deformation
y'	Length where temperature profile changes from uniform to normal distribution
r'	Radius where temperature profile changes from uniform to normal distribution
Λ	l/s, R/s
λ	y'/s, r'/s

Table A.2: Dimension-Related Symbols and Their Definitions

Material Properties	
α	Coefficient of thermal expansion
ν	Poisson Ratio
E	Young's Modulus
m	Weibull's Modulus
k	Heat conductivity
σ_e	Electrical conductivity
i_0	Exchange current density

Table A.3: Material-Properties-Related Symbols and Their Definitions

Stresses	
σ_{res}	Residual stress
$\sigma_{b,cr}$	Critical buckling stress
σ_{th}	Thermal stress
σ_p	Plate stress
σ_0	Reference stress
σ_1	Principal stress in 1-direction
σ_2	Principal stress in 2-direction
σ_3	Principal stress in 3-direction

Table A.4: Stress-Related Symbols and Their Definitions

Other Quantities	
S	Safety factor
P_f	Probability of failure
P_s	Probability of survival
V_0	Reference volume
V	Volume
A	Area
Q	Heat loss
q	Heat loss per unit plate area
E_0	Open circuit potential
η_{ohm}	Ohmic potential
$\eta_{act,a}$	Anode activation potential
$\eta_{act,c}$	Cathode activation potential
ρ_{H_2}	Partial pressure of hydrogen
ρ_{O_2}	Partial pressure of oxygen
ρ_{H_2O}	Partial pressure of water
ρ_0	Reference pressure
F	Faraday's constant
R_g	Gas constant
K_p	Equilibrium constant
i	Current per unit area
p	Power per unit area
p_{net}	$p - q$
p_{ave}	Average power per unit area

Table A.5: Other Symbols Used and Their Definitions

Bibliography

[1] A. Atkinson and A. Selık. Mechanical behavior of ceramic oxygen ion-conducting membranes. *Solid State Ionics 134 (2000) 59-66.*

[2] A. F. Jankowski, J. P. Hayes, R. T. Graff, and J. D. Morse. Micro-fabricated thin-film fuel cells for portable power requirements. volume 730. Material Research Society Symposium Proceedings.

[3] Discussions with C. Baertsch.

[4] C. Baertsch. Design strategies for a planar 2-sided SOFC. Power Point slides, March 17,2003. MURI Meeting.

[5] C. D. Baertsch, K. F. Jensen, J. L. Hertz, H. L. Tuller, S. T. Vengallatore, S. M. Spearing, and M. A. Schmidt. Fabrication and structural characterization of self-supporting electrolyte membranes for a micro solid-oxide fuel cell. For submission to Journal of Materials Research.

[6] Discussions with B. Chachuat.

[7] S. J. Chapman. *Fortran 90/95 for scientists and engineers.* WCB McGraw-Hill, first edition, 1998.

[8] K.-S. Chen. *Materials characterization and structural design of ceramic micro turbomachinery.* PhD thesis, Massachusetts Institute of Technology, 1998.

[9] Discussions during Weekly Microchemical Power Meeting.

[10] Discussions with J. Hertz.

[11] H. M. Jensen. Energy release rates and stability of straight-sided, thin-film delaminations. *Acta Metallurgica et Materialia Vol. 41, No. 2 pp. 601-607, 1993.*

[12] K. A. Murugesamoorthi, S. Srinivansan, and A. J. Appleby. *Fuel cell systems (L. J. M. J. Blomen and M. N. Mugerwa, editors)*, chapter 10, Research, development, and demonstration of solid oxide fuel cell systems. Plenum Press, 1993.

[13] K. F. Jensen. Microchemical Systems for fuel processing and conversion to electrical power. Interim Progress Report 3/01/02-3/31/03. OMB Number 0704-0188, Funding Number DAAD 19-01-1-0566, Sponsoring/Monitoring Agency Report Number 42236-CH-MUR, Massachusetts Institute of Technology, March 31, 2003. Sponsored/monitored by U.S. Army Research Office.

[14] L. R. Arana, S. B. Schaevitz, A. J. Franz, K. Jensen, and M. A. Schmidt. A microfabricated suspended-tube chemical reactor for fuel processing. IEEE MEMS 2002 Conference, January 20-24, Las Vegas, NV, U.S.A.

[15] M. F. Ashby, D. R. H. Jones. *Engineering materials 2 an introduction to microstructures, processing design.* Butterworth Heinemann, second edition, 1998.

[16] A. F. Mills. *Basic Heat & Mass Transfer.* Prentice Hall, second edition, 1999.

[17] Discussions with A. Mitsos.

[18] N. Nitani, T. Yamashita, T. Matsuda, S. -i. Kobayashi, and T. Ohmichi. Thermophysical properties of rock-like oxide fuel with spinel-yttria stabilized zirconia system. *Journal of Nuclear Materials 274 (1999) 15-22.*

[19] W. Nowacki. *Thermoelasticity.* Pergamon Press, 1986.

[20] Discussions by Professor D. M. Parks.

[21] Discussions with D. Quinn.

[22] R. R. Craig, Jr. *Mechanics of Materials.* John Wiley & Sons, 1996.

[23] R. J. Roark. *Roark's formulas for stress and strain/Warren C. Young.* McGraw-Hill, 1989.

[24] S. H. Chan, K. A. Khor, and Z. T. Xia. A complete polarization model of a solid oxide fuel cell and its sensitivity to the change of cell component thickness. *Journal of Power Sources 93 (2001) 130-140.*

[25] S. Srinivansan, B. B. Davé, K. A. Murugesamoorthi, A. Parthasarathy, and A. J. Appleby. *Fuel cell systems (L. J. M. J. Blomen and M. N. Mugerwa, editors)*, chapter 2, Overview of fuel cell technology. Plenum Press, 1993.

[26] W. S. Slaughter. *The linearized theory of elasticity.* Birkhäuser, 2002.

[27] Discussions with Professor S. M. Spearing.

[28] M. Spivak. *Calculus.* Publish or Perish, Inc., third edition, 1994.

[29] Discussions with V. T. Srikar.

[30] B. C. H. Stelle. Material science and engineering: The enabling technology for the commercialisation of fuel cell systems. *Journal of Material Science 36 (2001) 1053-1068.*

[31] J. Stewart. *Calculus Multivariable.* Brooks/Cole Publishing Company, third edition, 1995.

[32] W. A. Strauss. *Partial differential equations an introduction.* John Wiley & Sons, Inc., 1992.

[33] T. Y. A. Ie, K. T. Turner, V. T. Srikar, and S. M. Spearing. Analysis of the mechanical stability of fuel cell membranes, may 2003. Poster.

[34] T. Y. A. Ie, S. M. Spearing, V. T. Srikar, and K. Turner. Materials and structures issues in microchemical power devices, 2002. Poster. Data from Chelsey Baertsch, V. T. Srikar.

[35] Discussions with K. Turner.

[36] A. C. Ugural. *Stresses in plates and shells.* WCB McGraw-Hill, second edition, 1999.

[37] V. T. Srikar, K. T. Turner, T. Y. A. Ie, and S. M. Spearing. Structural design considerations for micromachined solid-oxide fuel cells. *Journal of Power Sources 125 (2004) 62-69.*

[38] W. D. Callister, Jr. *Material science and engineering an introduction.* John Wiley & Sons, Inc., fourth edition, 1997.

[39] Y. A. Çengel and M. A. Boles. *Thermodynamics an engineering approach.* WCB McGraw-Hill, third edition, 1998.